A Quantum Theory of the Biological Effects of Radio-frequencies and its application to Cancer

Vincent Lauer*

21 October 2013

Abstract

This paper proposes a scientific explanation of observed biological effects of exposure to artificial radio-frequency electromagnetic waves, based on transitions between different conformations which are stimulated by artificial electromagnetic waves and by the thermal electrical field. A first application predicts intensity-dependent peaks of a previously observed biological effect. In a second application , equations are derived that describe the inhibition by electromagnetic waves of the recognition of an antigen-presenting cell (APC) displaying a peptide-major histocompatibility complex (pMHC), by a T cell having a T Cell Receptor (TCR). Taking into account thymus selection of new T cells with or without exposure to an artificial electromagnetic wave, rules are derived that govern the effect of artificial electromagnetic waves on various classes of diseases. Theoretical predictions concerning cancer are found to be in agreement with death statistics, previous publications and past experimental results.

1 Introduction

The non-thermal effects of electromagnetic waves are generally the object of intense controversy [8] [7].

Concerning the effects of exposure to TV and FM radio on cancer, a number of statistical studies were made with different conclusions [20] [21] [6] [14] [28]. These studies concentrated on the distance between emitter and place of living as a parameter and found diverse results as to the correlation between this parameter and cancer death rates. None of these studies took into account the time between onset or increase in power of the emitter and cancer deaths.

Concerning the effect of cellular phones on their users a decreased incidence of brain cancer is found for moderate users [23] which is confirmed in [42] for latencies of more than 10 years, but is not confirmed in [27]. A short term increase of brain cancer incidence is found for heavy cellular phone users in [23] which is confirmed in [27] , except that in the case of analog cellular phone users the latency in [27] is very long.

Concerning cellular telephony base stations, [47] showed an increased overall cancer risk for persons living near a mobile phone base station.

Concerning therapeutic application of electromagnetic waves it was claimed that short-term exposure to a wideband electromagnetic wave could cure cancer [33] [41].

Possible effects on the immune systems have been considered. Early russian results were found non-confirmed [18] and were confirmed [22] by different teams, both teams using cw exposure systems.

One line of experimental results concerning non-thermal effects of electromagnetic waves on biological systems consistently yielded to the conclusion that these effects were dependent on the presence of both a static and an alternating magnetic field [12] [34]. A theory was developed to explain these results based on a quantum mechanical background and the analogy between these effects and cyclotron resonance [34]. This theory was criticized [9] but was also further developed yielding to an improved Ion Parametric Resonance (IPR) model in line with experimental results [13]. This IPR model applies to biological effects which depend on the existence of both a static and an alternating magnetic field, and generally has been applied only to very low frequency interactions. Other theories were also proposed [39] [24] [26] .

Generally, observed biological effects of electromagnetic waves, particularly on cancer, were given little credit. This is due to their apparent mutual inconsistency and, most importantly, to the absence of any reasonable scientific explanation [23] [42]. The aim of this paper is to propose a reasonable scientific explanation of observed biological effects, particularly concerning cancer. Unlike the IPR model, the proposed theory is not dependent on the existence of any static magnetic field, so that the addressed interactions differ from those addressed by the IPR model. A further aim of this paper is to provide additional statistical evidence confirming the proposed theory and allowing a first evaluation of the public health impact of exposure to artificial electromagnetic waves, specifically concerning cancer.

In this paper, a basic mechanism of interaction based on radiofrequency-induced transitions between two configurations of an elementary biological system yields equations predicting intensity-dependent peaks of a previously observed biological effect [19]. The TCR-pMHC interaction between a T Cell Receptor (TCR) and a Peptide - Major Histocompatibility Complex (pMHC) presented by an Antigen Presenting Cell (APC) is then modeled based on a plurality of successively adopted conformations. Quantum

*5 allée de l'Aire, 44240 La Chapelle sur Erdre, France
www.vincent-lauer.fr, contact@vincent-lauer.fr

equations governing the interaction are obtained, based on stimulated transitions between three conformations. These transitions are stimulated by the thermal electromagnetic field and/or the artificial electromagnetic waves. Under some restrictive hypotheses, the theory predicts that exposure to radiofrequencies can inhibit the recognition of a pMHC by a TCR. This inhibition also affects thymus selection of naive T cells, resulting in that after a transition from low to high exposure the normal behaviour of the immune system is reinstated after a latency period with respect to cancer and autoimmune diseases, but not with respect to pathogens or inflammatory diseases. This inhibition of TCR-pMHC recognition during thymus selection also results in an anti-cancer, pro-auto-immune effect of exposure to time-varying electromagnetic waves.

The temporary pro-cancer effect of the transition from low to high exposure is then confirmed by an abnormal variation of death rates following the onset of DVB-T which affected small cities having a DVB emitter but did not affect comparable cities that did not have a DVB emitter, and by cause of death statistics following the onset of DVB-T in Paris. This pro-cancer effect is also consistent with previous observations of increased cancer incidence near cell phone base stations in the few years immediately following onset of a base station [47].

The anti-cancer effect of exposure to time-varying electromagnetic waves is confirmed by a major drop of cancer as a cause of death in the 35-44 age class following the introduction of various communication networks causing time-varying exposure of the general population. It explains observed low brain cancer incidence in users of NMT or GSM cellular phones [23] [42]. It yields a rational explanation for the anti-cancer efficacy of temporary exposure to electromagnetic waves which was used for therapeutic purposes in the 1930s [33].

An interpretation of the high cancer rates in heavy users of GSM [23] [27] is also proposed based on the basic mechanism of radiofrequency-induced transitions between two configurations.

The quantum mechanical approach used in this paper is based on general knowledge on quantum mechanics [16]. Treatment of the interaction of electromagnetic waves with matter is semi-classical : waves are treated classically and biological elements are treated as quantum systems, in a way which closely parallels the semi-classical theory of atom-field interaction [37].

2 general calculation of transition probabilities between two conformations

I will initially consider any "elementary biological system" which can be for example a protein, an assembly of proteins, or other molecules including DNA or RNA.The elementary biological system will generally have a plurality of spatial configurations. For example, a protein may fold in different conform ations.

I model the elementary biological system using a set of coordinates typically representing atom positions, ignoring electronic transitions. This approach is generally

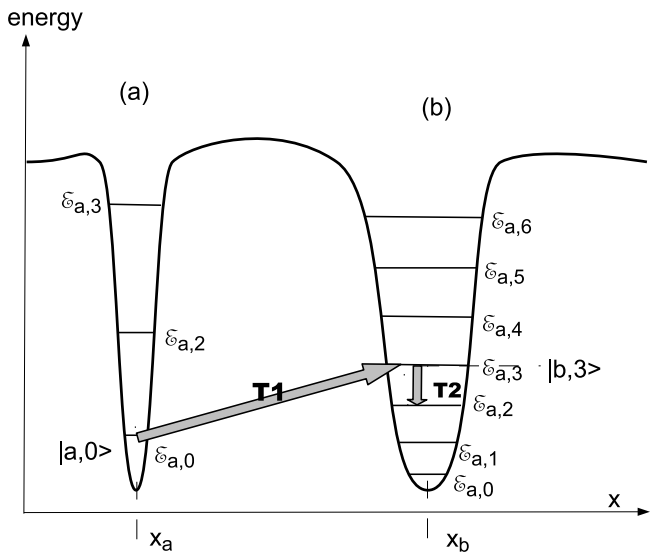

Figure 1: energy profile showing two quantum wells.

accepted for modelling vibrational levels of molecules, see for example the ammonia molecule in [16]. Ignoring electronic transitions is acceptable because electronic transitions generally correspond to energy differences significantly higher than vibrational energy differences or conformational energy differences.

Figure 1 shows a schematic representation of the energy variations of an elementary biological system, in a single-dimensional case. The vertical axis represents the energy $\mathscr{E}$, the horizontal axis represents a coordinate x. The curved line represents the conformational energy of the elementary biological system as a function of x. Although I represented a single degree of liberty x, this model in the general case has a plurality of degrees of liberty which I shall describe as a vector $\mathbf{x}$ in an s-dimensional coordinate space S. For example, a component of $\mathbf{x}$ can be a distance between two atoms of the elementary biological system or an angle between two parts of the elementary biological system which can rotate relative to each other.

The energy of the elementary biological system has two wells (a) and (b) respectively centred at $\mathbf{x}_a$ and $\mathbf{x}_b$. These wells correspond to distinct configurations (a) and (b) of the elementary biological system, respectively. In configuration (a) [resp. (b)] the wave function of the elementary biological system essentially has its non-zero values around x_a [resp. x_b], inside a bound portion I_a [resp. I_b] of the s-dimensional coordinate space S (in the one-dimensional case I_a and I_b are intervals).

In the represented one-dimensional case the quantum state of the elementary biological system in the potential well (a) may be any of the ground state $|a,0\rangle$ (having energy $\mathscr{E}_{a,0}$) or the first excited state $|a,1\rangle$ (having energy $\mathscr{E}_{a,1}$) or the second excited state $|a,2\rangle$(having energy $\mathscr{E}_{a,2}$). Each of these states represents a different vibrational level of the elementary biological system in well (a), and has been represented as a horizontal bar inside well (a), at a vertical position corresponding to its energy. Generally, I will note $|a,n\rangle$ [resp. $|b,n\rangle$] the n-th excited state (with $n = 0$ for the ground state) of the elementary biological system in quantum well (a) [resp. (b)] and $\mathscr{E}_{a,n}$ [resp.

$\mathscr{E}_{b,n}$] the energy of the elementary biological system in that quantum state.

If wells (a) and (b) were limited by infinitely high potential barriers, then an eigenfunction of the elementary biological system would be entirely within well (a) and another eigenfunction would be entirely within well (b). If the potential barriers have finite height, then assuming the energy levels in well (b) are different from the energy levels in well (a) (i.e. assuming that $\mathscr{E}_{a,n} \neq \mathscr{E}_{b,m}$ for all useful values of n, m) the finiteness of the potential barrier acts as a perturbation of each eigenfunction, so that the eigenfunctions $|a,n\rangle$ remain essentially unchanged within potential well (a) but acquire very small component in potential well (b). This small component is not an eigenfunction in potential well (b) and therefore there are at least some eigenfunctions in potential well (b) to which ones the small component is not orthogonal. As a result of this, the overlap

$$O_{a,n;b,m} = \int_{(I_a)} \phi_{a,n}(\mathbf{x})\phi^*_{b,m}(\mathbf{x})\,\mathrm{d}\mathbf{x} \tag{1}$$

is small but non-zero for at least some couples of eigenfunctions $|a,n\rangle$, $|b,m\rangle$ wherein $\mathscr{E}_{a,n} \neq \mathscr{E}_{b,m}$, with $\phi_{a,n}(\mathbf{x}) = \langle \mathbf{x}|a,n\rangle$, $\phi_{b,m}(\mathbf{x}) = \langle \mathbf{x}|b,m\rangle$.

Now I assume that the elementary biological system when in the configuration (a) [resp. (b)] has a (three-dimensional) electric dipole moment $\mathbf{d}(\mathbf{x}) = \mathbf{d}_a$ [resp. $\mathbf{d}(\mathbf{x}) = \mathbf{d}_b$] which is substantially constant over I_a [resp. I_b]. I also assume that the probability of presence $\langle \phi_{a,n}(\mathbf{x})|\phi_{a,n}(\mathbf{x})\rangle$ [resp. $\langle \phi_{b,m}(\mathbf{x})|\phi_{b,m}(\mathbf{x})\rangle$] is essentially concentrated in I_a [resp. I_b] with other non-zero values in I_b [resp. I_a] and is negligible everywhere else. Then:

$$\int_{(S)} \phi_{a,n}(\mathbf{x})\phi^*_{b,m}(\mathbf{x})\,\mathrm{d}^s\mathbf{x} = \int_{(I_a)} \phi_{a,n}(\mathbf{x})\phi^*_{b,m}(\mathbf{x})\,\mathrm{d}^s\mathbf{x} + \int_{(I_b)} \phi_{a,n}(\mathbf{x})\phi^*_{b,m}(\mathbf{x})\,\mathrm{d}^s\mathbf{x} = 0 \tag{2}$$

wherein the equality to zero is due to $|a,n\rangle$ and $|b,m\rangle$ being mutually orthogonal eigenfunctions.

and:

$$\int_{S} \phi_{a,n}(\mathbf{x})\mathbf{d}(\mathbf{x})\phi^*_{b,m}(\mathbf{x})\,\mathrm{d}^s\mathbf{x} = \mathbf{d}_a \int_{I_a} \phi_{a,n}(\mathbf{x})\phi^*_{b,m}(x)\,\mathrm{d}^s\mathbf{x} + \mathbf{d}_b \int_{I_b} \phi_{a,n}(\mathbf{x})\phi^*_{b,m}(\mathbf{x})\,\mathrm{d}^s\mathbf{x} \tag{3}$$

Combining equations 2 and 3 yields the three-dimensional electric dipole matrix element:

$$\mathbf{D}_{a,n;b,m} = \langle \phi_{a,n}|\mathbf{d}|\phi_{b,m}\rangle = \int_{(S)} \phi_{a,n}(\mathbf{x})\mathbf{d}(\mathbf{x})\phi^*_{b,m}(\mathbf{x})\,\mathrm{d}^s\mathbf{x} = (\mathbf{d}_a - \mathbf{d}_b)\int_{(I_a)} \phi_{a,n}(\mathbf{x})\phi^*_{b,m}(\mathbf{x})\,\mathrm{d}^s\mathbf{x} \tag{4}$$

Which can be written using the definition in equation (1):

$$\mathbf{D}_{a,n;b,m} = (\mathbf{d}_a - \mathbf{d}_b)O_{a,n;b,m} \tag{5}$$

The individual components of this dipole matrix element are the matrix elements of the projections of the dipole moment on each axis.

The dipole matrix element $\mathbf{D}_{a,n;b,m}$ between the eigenstates $|a,n\rangle$ and $|b,m\rangle$ is thus proportional to the difference between the dipole moments in each conformation, and to the overlap on a single quantum well between the two eigenstate wave functions. When the overlap is non-zero and there is a difference between the elementary biological system's dipole moments in each conformation, then there will be a non-zero transition dipole matrix element and thus a transition between the two eigenstates $|a,n\rangle$ and $|b,m\rangle$ is allowed which can yield stimulated transitions when the elementary biological system is exposed to an electromagnetic field of frequency $\nu = \frac{1}{h}|\mathscr{E}_{a,n} - \mathscr{E}_{b,m}|$. An example of an allowed transition from $|\phi_{a,0}\rangle$ to $|\phi_{b,3}\rangle$ is represented on figure 1 as T. This transition brings the elementary biological system from configuration (a) to configuration (b) despite the existence of the potential barrier, in a manner analogous to the quantum tunneling effect.

When the elementary biological system is submitted to a time-varying electric field $\mathbf{E}\cos\omega t$ the matrix element of the interaction hamiltonian between the elementary biological system and the field is :

$$\langle a,n|H_{int}|b,m\rangle = \mathbf{D}_{a,n;b,m}\cdot\mathbf{E}\cos\omega t \tag{6}$$

wherein $\cdot$ denotes the scalar product.

When interacting with the field the elementary biological element undergoes Rabi oscillations between states $|a,n\rangle$ and $|b,m\rangle$ and the frequency of these transitions is the Rabi frequency

$$\Omega_{a,n;b,m} = \frac{1}{\hbar}\mathbf{E}\cdot\mathbf{D}_{a,n;b,m} \tag{7}$$

This equation may also be written:

$$\Omega_{a,n;b,m} = \frac{1}{\hbar}\mathbf{E}\cdot(\mathbf{d}_a - \mathbf{d}_b)O_{a,n;b,m} \tag{8}$$

In the following sections the indices n, m will often be implied rather than expressly written in equation 7. With this convention equations 5 and 7 yield respectively :

$$\mathbf{D}_{a;b} = (\mathbf{d}_a - \mathbf{d}_b)O_{a;b} \tag{9}$$

$$\Omega_{a;b} = \frac{1}{\hbar}\mathbf{E}\cdot\mathbf{D}_{a;b} \tag{10}$$

3 equivalent RMS Rabi frequencies

Rabi frequencies governing transitions stimulated by the electromagnetic field are usually defined for single mode electromagnetic waves. However, electromagnetic waves which are not single mode can also cause stimulated transitions between quantum states. In this section I discuss a simple approximation which facilitates the evaluation

of transitions stimulated by electromagnetic waves which have an extended frequency spectrum. This approximation is based on the use of equivalent Rabi frequencies which have the same role which Rabi frequencies have for single mode waves.

3.1 single mode frequency range

I first consider only a single mode electromagnetic wave with a frequency shift $\Delta\omega$ with respect to the resonance of an $|a\rangle$ to $|b\rangle$ transition between wells (a) and (b) (for simplicity I now omit the indexation of the energy states within each quantum well). The Rabi frequency of the $|a\rangle$ to $|b\rangle$ transition for the electric field amplitude of this single mode wave is Ω_S. The inversion (probability of finding the system in state $|a\rangle$ minus probability of finding the system in state $|b\rangle$) is (see for example section 5.2 of [37]) : $\frac{(\Delta\omega)^2-\Omega_S^2}{(\Delta\omega)^2+\Omega_S^2}\sin^2\left(\frac{1}{2}\sqrt{(\Delta\omega)^2+\Omega_S^2}\right)+\cos^2\left(\frac{1}{2}\sqrt{(\Delta\omega)^2+\Omega_S^2}\right)$ which can also be written $\frac{(\Delta\omega)^2}{(\Delta\omega)^2+\Omega_S^2}+\frac{\Omega_S^2}{(\Delta\omega)^2+\Omega_S^2}\cos(\sqrt{(\Delta\omega)^2+\Omega_S^2})$. The amplitude of the variable part is $\frac{\Omega_S^2}{(\Delta\omega)^2+\Omega_S^2}$. The full width at half maximum (FWHM) of this amplitude as a function of $\Delta\omega$ is $2\Omega_S$. In a first approximation, the only frequencies that contribute to stimulated absorption and emission are thus within a frequency range of $2\Omega_S$.

3.2 equivalent Rabi frequency and Rabi integration bandwidth

Now I consider an electromagnetic wave which is a flat Gaussian noise having a spectral power S_{tot} near the resonant frequency of the $|a\rangle$ to $|b\rangle$ transition, and which electric field is parallel to the three-dimensional electric dipole matrix element $\mathbf{D}_{a;b}$ corresponding to the $|a\rangle$ to $|b\rangle$ transition.

The RMS value E_{tot} of the electric field in a small angular frequency range $\delta\omega$ centred on the resonant frequency of the $|a\rangle$ to $|b\rangle$ transition is related to the bandwidth and spectral power by:

$$S_{tot}\frac{\delta\omega}{2\pi}=\frac{E_{tot}^2}{c\mu_0} \tag{11}$$

The RMS Rabi frequency of the $|a\rangle$ to $|b\rangle$ transition for a field E_{tot} parallel to $\mathbf{D}_{a;b}$ is, from equation 10:

$$\Omega_{tot}=\frac{1}{\hbar}D_{ab}E_{tot} \tag{12}$$

with $D_{ab}=|\mathbf{D}_{a;b}|$.

In a simple approximation, only a central frequency slot of the electromagnetic wave centred on the resonant frequency of the $|a\rangle$ to $|b\rangle$ transition, has a significant role in $|a\rangle$ to $|b\rangle$ stimulated transitions. The bandwidth of this frequency slot is a "Rabi integration bandwidth" $\delta\omega$ corresponding to the frequency range $2\Omega_S$ obtained in section 3.1, in which Ω_{tot} now replaces Ω_S:

$$\delta\omega=2\Omega_{tot} \tag{13}$$

This bandwidth is also equal to the bandwidth on which the power is integrated in equation 11 for the purpose of obtaining the RMS Rabi frequency Ω_{tot}, so that equations 11, 12 and 13 can be combined, yielding:

$$\Omega_{tot}=2\mu_0 c\frac{D_{ab}^2}{\hbar^2}\frac{S_{tot}}{2\pi} \tag{14}$$

The RMS Rabi frequency of the $|a\rangle$ to $|b\rangle$ transition for the part of the electric field which stimulates $|a\rangle$ to $|b\rangle$ transitions ("equivalent RMS Rabi frequency") is thus given by equation 14. This approximation is only valid when the Rabi integration bandwidth - which is twice the Rabi frequency as per equation 13 - remains small compared to the overall bandwidth of the electromagnetic wave.

3.3 thermally stimulated transitions

The effects of artificial electromagnetic waves on transitions between quantum states of the elementary biological system must be compared to the likelihood of such transitions occurring naturally. Such transitions may occur naturally by spontaneous decay or because the thermal electromagnetic field stimulates transitions.

From Planck's law the thermal spectral power per unit area in a solid angle corresponding to a half space and in an angular frequency range $\delta\omega$ around the center frequency ω is (for small ω):

$$S_{th}=\frac{1}{(2\pi)}\frac{\omega^2}{c^2}kT \tag{15}$$

wherein k is Boltzmann's constant, T is the temperature in Kelvins.

The RMS value E_{th} of the thermal electric field along an arbitrary direction in a frequency range $\delta\omega$ is related to the thermal power per unit area by:

$$S_{th}\frac{\delta\omega}{2\pi}=\frac{E_{th}^2}{c\mu_0} \tag{16}$$

Equation 16 corresponds to equation 11 and the equivalent Rabi frequency (or thermal Rabi frequency Ω_{th})can thus be obtained by substituting S_{th} to S_{tot} in equation 14 yielding:

$$\Omega_{th}=2\frac{1}{(2\pi)^2}c\mu_0 kT\left(\frac{\omega D_{ab}}{\hbar c}\right)^2 \tag{17}$$

3.4 artificial wave superimposed on the thermal electric field

I assume that an artificial electromagnetic wave superimposed on the thermal electric field has an electric field parallel to the three-dimensional electric dipole matrix element $\mathbf{D}_{a;b}$. In this case the equivalent Rabi frequency is obtained by substituting $S_{art}+S_{th}$ in equation 14, wherein S_{art} is the spectral power of the artificial wave, yielding:

$$\Omega_{tot}=2\mu_0 c\frac{D_{ab}^2}{\hbar^2}\frac{S_{art}+S_{th}}{2\pi} \tag{18}$$

3.5 dominance of thermally stimulated transitions over spontaneous decay

I will momentarily use a thermal bandwidth Γ_{th} which is the inverse of the lifetime of an initial pure state (a or b) and is thus one quarter of the equivalent RMS Rabi frequency:

$$\Gamma_{th} = \frac{2}{4(2\pi)^3} c\mu_0 kT \left(\frac{\omega D_{ab}}{\hbar c}\right)^2 \tag{19}$$

This thermal bandwidth compares with the spontaneous decay bandwidth which is [37]:

$$\Gamma_{spont} = \frac{\omega^3 D_{ab}^2}{3\pi\epsilon_0 c^3 \hbar} \tag{20}$$

I can thus calculate

$$\frac{\Gamma_{spont}}{\Gamma_{th}} = \frac{4(2\pi)^2}{3} \frac{1}{\mu_0\epsilon_0 c^2} \frac{\hbar\omega}{kT} \tag{21}$$

This value is 1 when the angular frequency ω is :

$$\omega_{trans} = \frac{3}{4(2\pi)^2} \mu_0\epsilon_0 c^2 \frac{kT}{\hbar} \tag{22}$$

$\frac{\omega_{trans}}{2\pi}$ is about 120 GHz. Below this, stimulated thermal emission - absorption between a higher energy state and a lower energy state dominate over spontaneous decay from the higher energy to the lower energy state. This is the case for all radiofrequencies of interest. Therefore spontaneous decay will generally be ignored herein and transition probabilities will be calculated based on stimulated transitions only.

4 a basic mechanism of interaction between an artificial electromagnetic wave and an elementary biological system

4.1 description of the basic interaction mechanism

I now consider an elementary biological system (for example a protein) having two conformations corresponding to quantum wells (a) and (b) as shown on figure 1, separated by energy barriers much higher than any occupied energy level. I will limit the analysis to the states $|a,n\rangle$, $|b,m\rangle$, $|b,m-1\rangle$, for example with $n=0, m=3$ as illustrated on figure 1. The allowed transitions are from $|a,n\rangle$ to $|b,m\rangle$ (T1 on figure 1) and from $|b,m\rangle$ to $|b,m-1\rangle$ (T2 on figure 1). The system is initially in state $|a,n\rangle$ at $t=0$. The frequencies of interest are below 60 GHz so the dominant natural transitions are thermally stimulated transitions. There is an artificial electromagnetic wave at the resonant frequency of the transition T1 from $|a,n\rangle$ to $|b,m\rangle$, and the transition T2 from $|b,m\rangle$ to $|b,m-1\rangle$ is thermally stimulated. The Hamiltonian in the interaction picture is:

$$V = -\frac{\hbar}{2}\left(\Omega_{art}|b,m\rangle\langle a,n| + \Omega_{art}^*|a,n\rangle\langle b,m| + \Omega_{th2}|b,m\rangle\langle b,m-1| + \Omega_{th2}^*|b,m-1\rangle\langle b,m|\right) \tag{23}$$

wherein the Rabi frequency $\Omega_{art} = \Omega_{a,n;b,m}$ is calculated as per equation 7 for the electric field E of the artificial electromagnetic wave, and Ω_{th2} is a Rabi frequency of thermally stimulated transitions between states $|b,m\rangle$ and $|b,m-1\rangle$. Solving the equations of motion $\frac{\partial}{\partial t}|\phi(t)\rangle = -\frac{i}{\hbar}V|\phi(t)\rangle$ for a system initially in state $|\phi(0) = |a,n\rangle$ yields the state vector at time t (adapted from [37]):

$$\begin{aligned}|\phi(t) >= i\frac{\Omega_{art}}{\Omega_{av}} \sin\left(\frac{\Omega_{av}t}{2}\right)|b,m\rangle \\ + \left[\frac{\Omega_{th2}^2}{\Omega_{av}^2} + \frac{\Omega_{art}^2}{\Omega_{av}^2}\cos\left(\frac{\Omega_{av}t}{2}\right)\right]|a,n\rangle \\ - \frac{\Omega_{th2}\Omega_{art}}{\Omega_{av}^2}\left[1+\cos\left(\frac{\Omega_{av}t}{2}\right)\right]|b,m-1\rangle\end{aligned} \tag{24}$$

with: $\Omega_{av} = \sqrt{\Omega_{th2}^2 + \Omega_{art}^2}$

Assuming $\Omega_{art} >> \Omega_{th2}$, the coefficient of $|b,m-1>$ remains near zero whilst the coefficient of $|b,m>$ increases from zero at $t=0$ to $-i$ at $t=\frac{1}{2\Omega_{av}}$. For $\Omega_{art} >> \Omega_{th2}$ equation 24 is equivalent to:

$$\begin{aligned}|\phi(t)\rangle = i\frac{\Omega_{art}}{|\Omega_{art}|}\sin\left(\frac{|\Omega_{art}|t}{2}\right)|b,m\rangle \\ + \cos\left(\frac{|\Omega_{art}|t}{2}\right)|a,n\rangle\end{aligned} \tag{25}$$

I assume that the artificial wave is a square pulse of duration $T_{pulse} = \frac{\pi}{\Omega_{art}}$ repeated periodically, with two successive pulses being separated by a time interval T_{step}. Between 0 and T_{pulse} the system is governed by equation 25 so $|\phi(T_{pulse})\rangle = i\frac{\Omega_{art}}{|\Omega_{art}|}|b\rangle$. The pulse can thus cause a transition to occur between the two quantum states $|a\rangle$ and $|b\rangle$.

4.2 example of a detailed mechanism based on conformation change

I now assume that absent the artificial wave the transitions between the two quantum wells can be neglected; in particular the electric field of thermal origin which exists even in the absence of the artificial wave is insufficient to cause significant transitions to occur between the two quantum wells. I further assume that during T_{step} thermal relaxation occurs within each quantum well separately, i.e. for example transitions do occur between $|b,m\rangle$ and $|b,m-1\rangle$ or $|b,m+1\rangle$, and between $|a,n\rangle$ and $|a,n-1\rangle$ or $|a,n+1\rangle$

The interaction thus comprises two steps:

- in a first step ($t=0$ to $t=T_{pulse}$) the conformation of the elementary biological system changes, more precisely the quantum state of the elementary biological system changes from $|a\rangle$ to $|b\rangle$.

- in a second step (from $t=T_{pulse}$ to $t=T_{pulse}+T_{step}$) thermal relaxation makes the system change its quantum

state within quantum well (a) and within quantum well (b) separately.

Now I assume that the interval between pulses T_{step} is sufficient to allow for thermal relaxation both within quantum well (a) and within quantum well (b), and I consider a statistical mixture of quantum states which initially are all within the quantum well (a) and have a thermal distribution between quantum states inside that quantum well.

- during the first step of the interaction all elementary biological elements which are in quantum state $|a,n\rangle$ enter quantum state $|b,m\rangle$. However at the end of the first step there is no more elementary biological system in state $|a,n\rangle$ within well (a) and all elementary biological systems in well (b) are in state $|b,m\rangle$. This is because during the first step there is no thermal relaxation within well (b): assuming $\Omega_{art} >> \Omega_{th2}$ the dominating coefficient $\frac{\Omega_{th2}\Omega_{art}}{\Omega_{av}^2}$ of $|b,m-1\rangle$ in equation 24 is a lot lower in the presence of the artificial wave than absent the artificial wave, so that thermal relaxation within well (b) is effectively prevented during the first step.

- during the second step of the interaction, elementary biological systems change their quantum states to come back to thermal equilibrium distribution separately within each quantum well. In particular, the absence of the artificial electric field during the second step allows thermal relaxation to proceed normally rather than be prevented as is the case during the first step. Therefore, the number of elementary biological systems which are in state $|a,n\rangle$ increases and almost comes back to its initial value, and the number of elementary biological systems which are in state $|b,m\rangle$ decreases and, if sufficient time is available, almost comes back to zero since these systems are spread over all quantum states of quantum well (b).

As the pulse is repeated this process also repeats until the two quantum wells are at thermal equilibrium between each other. At that point, transitions from quantum well (a) to quantum well (b) roughly equilibrate reverse transitions from quantum well (b) to quantum well (a).

In a biological organism, each elementary biological system (for example a protein) has a precise role which is determined by its conformation, i.e. its spatial arrangement, assuming that the chemical bonds are not affected. The statistical distribution of the conformations of a given type of elementary biological system is not determined by thermal laws but by biological processes, to say it otherwise it is determined by chemical kinetics rather than thermal equilibrium. After sufficiently numerous pulses have passed, the above mechanism can modify the statistical distribution of a given type of biological system from single-conformation to multi-conformation in thermal equilibrium, and this modified statistical distribution will then remain unchanged even if the pulse train is stopped, unless another biological process can correct it which is not necessarily the case. The pulse train of artificial electromagnetic wave has thus durably modified the statistical distribution of conformations of the investigated type of elementary biological systems. If the elementary biological system in its configuration (a) has a useful biological function which it does not have in its configuration (b), the behaviour of the biological organism can be strongly perturbated. A simple example of this is the prion protein [17] : a repeated pulse of appropriate duration and frequency could potentially change the normal prion protein PrP^C into the disease-causing isoform PrP^{Sc}. Whilst the prion conformations may or may not be "switchable" by a GSM pulse, action of the pulse on a less well-known protein having two distinct conformations probably caused the biological effect in [19].

The evolution of the elementary biological system after a stimulated transition from well (a) to well (b) is not necessarily determined exclusively by thermal relaxation within well (b). Quantum well (b) may also be an intermediate configuration from which further transformations occur faster than thermal relaxation inside the well. A number of detailed mechanisms are thus conceivable based on transitions between two conformations which are stimulated by pulses of an artificial electromagnetic wave.

4.3 power dependency of the basic mechanism

In the first step of interaction, i.e. during the pulse, the elementary biological system changes its conformation. This first step is governed by equation 25 and the general condition for this first step to bring about a full conformational change for an elementary biological system initially in state $|a,n\rangle$ is:

$$\frac{\Omega_k}{2}T_{pulse} = \frac{\pi}{2} + \pi k \tag{26}$$

with k an integer and Ω_k a Rabi frequency Ω_{art} corresponding to the index k. When equation 26 is verified, at the end of the pulse the elementary biological system which was initially in state $|a,n\rangle$ is in state $|b,m\rangle$, i.e. the conformational change is maximal and any biological effects should also peak. Otherwise, the conformational change is partial or absent and the biological effect is thus lower. Thus, the biological effects peaks for a series of values of Ω_k determined by equation 26. Ω_k is the Rabi frequency at the k-th peak of biological activity.

For an electric field parallel to the electric dipole moment the Rabi frequency is:

$$\Omega_k = \frac{1}{\hbar}D_{ab}\sqrt{c\mu_0 P_k} \tag{27}$$

wherein P_k is the peak power of the artificial wave at the k-th maximum of biological activity, and $D_{ab} = |\mathbf{D}_{a,n;b,m}|$ is the dipole matrix element between the two states $|a,n\rangle$ and $|b,m\rangle$ between which ones the transition occurs.

To fully cover practical applications, the case must be considered in which the artificial wave is not exactly resonant with the transition, but instead is offset from the transition frequency by a frequency shift δ.

in this case, the Rabi frequency is changed [37] from Ω_k to $\sqrt{\Omega_k^2 + \delta^2}$ in equation 26 yielding:

$$\frac{T_{pulse}^2}{\pi^2}\left(\delta^2 + \frac{c\mu_0}{\hbar^2}P_k D_{ab}^2\right) = (1+2k)^2 \tag{28}$$

The reduced variables $\delta_r = \frac{T_{pulse}}{\pi}\delta$ and $d_r = \frac{T_{pulse}}{\pi}\frac{\sqrt{c\mu_0}}{h}D_{ab}$ are introduced so that the equation can be written:

$$\delta_r^2 + P_k d_r^2 = (1+2k)^2 \tag{29}$$

Writing this equation for two different indices n and k yields:

$$\delta_r^2 = \frac{P_k(1+2n)^2 - P_n(1+2k)^2}{P_k - P_n} \tag{30}$$

now applying it with n=0:

$$P_k = \frac{-\delta_r^2 + (1+2k)^2}{-\delta_r^2 + 1} P_0 \tag{31}$$

Since P_k is necessarily positive, I also obtain:

$$0 \leq \delta_r^2 \leq 1 \tag{32}$$

4.4 experimental confirmation of the basic mechanism

The above equations apply to the results shown in [19] in its figure 1. This figure shows that the effect of GSM exposure peaks at $P_n = 10\mu W/cm2$ and $P_{n+1} = 378\mu W/cm2$ with no other peak between them. The GSM signal comprising pulses, the results from the previous section can be applied quite directly.

Now assuming that $n = 1$, using formula 30 the value $\delta_r^2 = 8.56$ is obtained, which is incompatible with inequality 32 so that solution can be excluded. Assuming $n = 0$ the value $\delta_r^2 = 0.78$ is obtained, which is compatible with inequality 32 . This explains why no other peak has been obtained for powers below $P_0 = 10\mu W/cm2$ corresponding to distances larger than 30 cm on the figure: this peak is the first, lowest-power one, in the series.

Similar considerations do apply to the results shown on figure 2 of the same publication. In this case $\delta_r^2 = 0.63$, $P_0 = 11\mu W/cm2$, $P_1 = 252\mu W/cm2$.

The experimental verification of the power dependency of equation 31 in the experiments of [19] is confirmation that the mechanism of section 4.1 is the underlying cause of the biological effects described in [19].

4.5 comparison of naturally occurring transitions with GSM-stimulated transitions

Whenever the transition frequency is below 120 GHz, the only way in which the transition described in section 4.4 can happen naturally is by thermally stimulated transition. When the transition is stimulated by an artificial wave parallel to the electric dipole moment, the shortest pulse duration which yields a complete transition is $\tau_{art} = \frac{\pi}{2\Omega_{art}}$ wherein $\Omega_{art} = \Omega_{a,n;b,m}$ is calculated based on equation 7, yielding:

$$\tau_{art} = \frac{\pi}{2} \frac{\hbar}{D_{ab}} \frac{1}{\sqrt{c\mu_0 P_{art}}} \tag{33}$$

wherein P_{art} is the power per unit area of the artificial wave and $D_{ab} = |\mathbf{D}_{a,n;b,m}|$ is the modulus of the electric dipole matrix element between the two quantum states $|a,n\rangle$ and $|b,m\rangle$.

When the transition is thermally stimulated a typical transition time is $\tau_{th} = \frac{\pi}{2\Omega_{th}}$ wherein Ω_{th} is given by equation 17. Combining equations 33 with 17 yields :

$$\tau_{th} = 4\pi\tau_{art}^2 \frac{c^2}{\omega^2} \frac{P_{art}}{kT} \tag{34}$$

When applied to GSM with τ_{art} =0.56 ms and P_{art} =0.1 W/m2 corresponding to the values in [19] the obtained value is τ_{th} =8 thousand years.

Thus, the transitions which causes the observed biological effect in [19] do never happen naturally as stimulated transitions through the direct path, and possibly never happen naturally at all. This fact also favours the conceptual possibility of the mechanism described in section 4.7.

4.6 compatibility with known dipole moments of proteins

The minimum pulse length which can trigger the transition is $T_{min} = \frac{\pi}{\Omega_{a,n;b,m}}$ with $\Omega_{a,n;b,m}$ as given by equation 8. When T_{min} is known this can be inversed as:

$$0_{a,n;b,m} = \frac{h}{2T_{min}|d_a - d_b|\sqrt{c\mu_0 P_{art}}} \tag{35}$$

An order of magnitude of the electric dipole moments is $1.6 \cdot 10^{-29}$C.m for a single amino acid residue (alanine) to $5.2 \cdot 10^{-28}$C.m for a 40-residue polyalanine [36]. This is also an order of magnitude for the difference $|d_a - d_b|$ between the dipole moments in different conformations for simple proteins. I take a reasonable $|d_a - d_b| = 10^{-28}$C.m. and $P_{art} = 0.1$ W/m2 which is approximately the value of P_0 corresponding to the experimental results in [19]. For $T_{min} = 5.4 \cdot 10^{-7}$s corresponding to GSM the calculated overlap is $O_{a,n;b,m} = 10^{-3}$. This is a reasonably low overlap value, as expected. Thus, usual values of the dipole moment for proteins are fully compatible with the present basic mechanism.

4.7 mechanisms which modifiy the chemical bonds

The coordinate $\mathbf{x}$ has been assumed to generally represent atom coordinates. Whilst mere changes of conformation which do not affect chemical bonds are expected to happen more easily due to lower energy barrier between the quantum wells, the mechanism may also conceivably allow transitions that modify chemical bonds. Quantum well (b) may thus be a state in which the chemical bonds have been modified as compared with quantum well (a), with typically one or more chemical bonds being replaced by other chemical bonds, with the overall energy of the elementary biological system being little modified, so that a radio-frequency electromagnetic wave can cause the transition. In such case the mechanism allows for a modification of the chemical bonds without the need to bring in the energy necessary for separately undoing a chemical bond and forming a new chemical bond.

DNA has a capacity to accumulate large dipole moments [31] [43] [5], which increases the Rabi frequencies and generally favours the mechanism of interaction described in this section. This capacity of accumulating large dipole moments makes DNA potentially more likely to undergo changes in its chemical structure when exposed

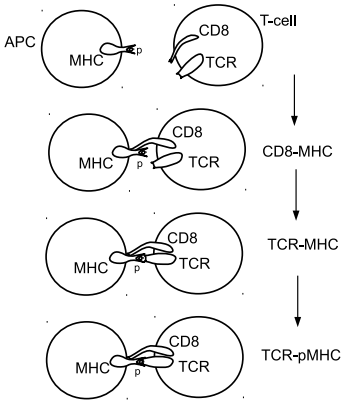

Figure 2: steps of the interaction between a T-cell and an Antigen Presenting Cell (APC)

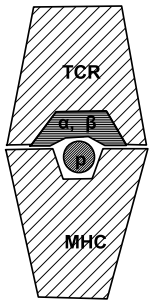

Figure 3: a T Cell Receptor (TCR) bound to a p-MHC (a complex of an antigen (p) and a Major Histocompatibility Complex molecule (MHC)

to a pulsed electromagnetic wave, as compared to other molecules which lack this capacity. This could conceivably cause mutations in DNA exposed to pulsed electromagnetic waves.

5 TCR-pMHC interaction

A key step of the immune response is the detection by the T cell receptor (TCR) of T lympphocytes, of foreign peptides (p) bound to major histocompatibility complex molecules (MHC; p-MHC being the complex of p and MHC) on the surface of antigen presenting cells (APCs).

There are three steps in the TCR/pMHC recognition as shown on figure 2:

First (step CD8-MHC) the CD8 co-receptor molecule binds to the MHC.

Then (step TCR-MHC) the TCR binds to the MHC.

Finally (step TCR-pMHC) the recognition occurs, i.e. the TCR-pMHC system undergoes a transition from a relatively weakly bound state to a strongly bound state.

Figure 3 shows a schematic of the TCR-pMHC system. The TCR binds to the MHC directly and has hypervariable regions α and β which are specific to one peptide p.

Figure 4C of [40] illustrates the general shape of the energy variations in the pMHC-TCR along a minimal energy line. I reproduce it on figure 4 with some variations.

In the CD8-MHC binding step, the CD8-pMHC-TCR assembly moves from a fully unbound state to a bound

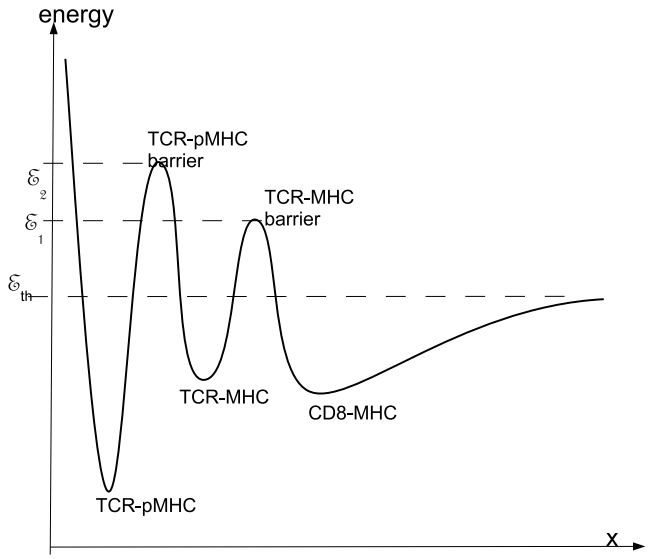

Figure 4: energy profile along a minimum energy line of the interaction of a T cell with an APC

state. There is no strong energy barrier separating the unbound state from this CD8-MHC bound state and the number of CD8-MHC which are in a bound state at any given time is probably ruled by thermal equilibrium. There is a minimum of the potential energy corresponding to the bound state and therefore there are more quantum states located around this minimum than anywhere else, and on average the T-cell and the APC are found more often "side by side" than they would be without this binding.

In the TCR-MHC binding step, the system gets into the TCR-MHC potential well as shown on figure 4. The energy barrier separating the TCR-MHC potential well from the CD8-MHC energy minimum has a maximum potential energy $\mathscr{E}_1 > \mathscr{E}_{th}$ wherein $\mathscr{E}_{th}$ denotes a maximum energy of the TCR-pMHC system at thermal equilibrium. The existence of this energy barrier stabilizes the TCR-MHC bound state.

In the TCR-pMHC binding step, the system gets into the TCR-pMHC potential well as shown on figure 4. The energy barrier separating the TCR-pMHC potential well from the TCR-MHC potential well has a maximum potential energy $\mathscr{E}_2 > \mathscr{E}_{th}$.

In order for the CD8 T-Cell to kill the APC the TCR-pMHC bound state must be maintained for a sufficient time.

The considerations in section 2 apply. Section 4 does not apply because there are already natural transitions between each quantum well. I will examine how these natural transitions are prevented by an artificial electromagnetic wave, rather than caused by an artificial electromagnetic wave as is the case in section 4.

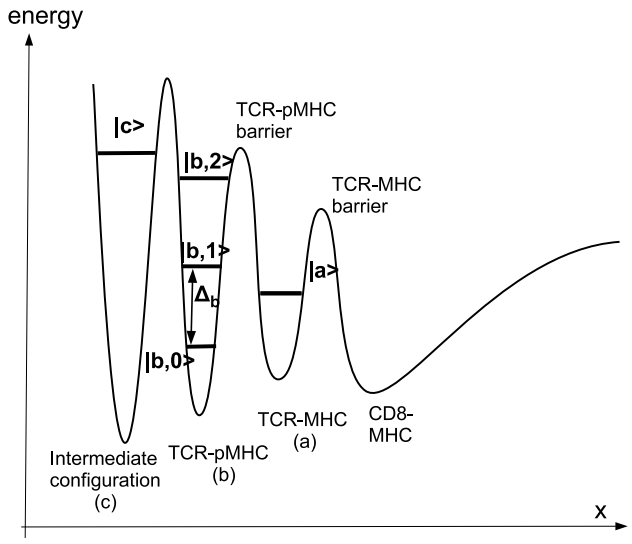

Figure 5: Energy profile along a minimum energy line of the interaction of a T cell with an APC, showing quantum energy levels in each well.

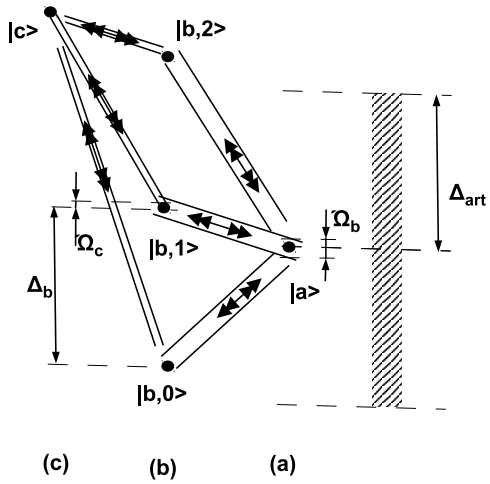

Figure 6: quantum transitions between quantum wells (a) (b) and (c). Each quantum state in each well is shown as a black dot.

6 pMHC-TCR interaction in the presence of an artificial electromagnetic wave

6.1 basic model

Figure 5 shows a final step of the T cell - APC interaction. I hypothesize that once the p-MHC-TCR-CD8 assembly is in the bound configuration corresponding to the quantum well labelled "TCR-pMHC", it moves to an intermediate configuration from which it will start a series of steps ultimately yielding to the destruction of the APC. This intermediate configuration is shown as a further quantum well (c) on figure 5. This step may involve the TCR-pMHC alone, or it may additionally involve some further constituent of the T cell.

Initially (after the TCR-MHC binding step) the system is in a quantum state $|a\rangle$ in the TCR-MHC quantum well (which is noted "well (a)" herein). It "then" binds, getting into any of the quantum states $|b,i\rangle$ in quantum well TCR-pMHC (well (b)), from which it starts a final reaction step, getting into quantum state $|c\rangle$ in a third well (c) representing the intermediate configuration. I assume that there is a single quantum state implied in well (c) but a plurality of quantum states implied in well (b) as shown on figure 5. Ω_{bi} is the Rabi frequency of the $|a\rangle$ to $|b,i\rangle$ transition and Ω_{ci} is the Rabi frequency of the $|b,i\rangle$ to $|c\rangle$ transition. Figure 6 illustrates this and shows transitions stimulated by the artificial wave as thicker, corresponding to larger Rabi frequencies, than transitions which are thermally stimulated and have smaller Rabi frequencies. The system may go from well (a) to well (c) via any of the quantum states in well (b) as shown on figure 6. Ω_{bi} and Ω_{ci} are generally complex numbers. The interaction picture Hamiltonian in the rotating wave approximation is:

$$V = -\frac{\hbar}{2}\sum_i (\Omega_{bi}|b,i\rangle\langle a| + \Omega_{bi}^*|a\rangle\langle b,i| + \Omega_{ci}|c\rangle\langle b,i| + \Omega_{ci}^*|b,i\rangle\langle c|) \quad (36)$$

The * denotes the complex conjugate. I use the notations:

$$S = \Omega_{b1}\Omega_{c1} + \Omega_{b2}\Omega_{c2} + \cdots + \Omega_{bn}\Omega_{cn} \quad (37)$$

$$R = -|\Omega_{b1}|^2 - |\Omega_{b2}|^2 - \cdots - |\Omega_{bn}|^2 + |\Omega_{c1}|^2 + |\Omega_{c2}|^2 + \cdots + |\Omega_{cn}|^2 \quad (38)$$

$$G = |\Omega_{b1}|^2 + |\Omega_{b2}|^2 + \cdots + |\Omega_{bn}|^2 \quad (39)$$

$$X^2 = \frac{R}{2} + G \quad (40)$$

$$Y^4 = S^2 + \frac{R^2}{4} \quad (41)$$

I note ω an eigenvalue of $-\frac{2}{\hbar}V$ and $|\psi\rangle = \alpha|a\rangle + \beta_1|b,1\rangle + \cdots + \beta_n|b,n\rangle$ a corresponding eigenvector. The eigenvalue equation $-\frac{2}{\hbar}V|\psi\rangle = \omega|\psi\rangle$ yields:

$$\begin{aligned}
&\Omega_{b1}^*\beta_1 + \Omega_{b2}^*\beta_2 + \cdots + \Omega_{bn}^*\beta_n = \omega\alpha \\
&\Omega_{c1}\beta_1 + \Omega_{c2}\beta_2 + \cdots + \Omega_{cn}\beta_n = \omega\gamma \\
&\Omega_{b1}\alpha + \Omega_{c1}^*\gamma = \omega\beta_1 \\
&\Omega_{b2}\alpha + \Omega_{c2}^*\gamma = \omega\beta_2 \\
&\vdots \\
&\Omega_{bn}\alpha + \Omega_{cn}^*\gamma = \omega\beta_n
\end{aligned} \quad (42)$$

Solving for ω yields a second-degree equation in ω^2 which has the solutions

$$\omega^2 = X^2 \pm Y^2 \quad (43)$$

so the eigenvalues are :

$$\omega_{\epsilon_1,\epsilon_2} = \epsilon_1\sqrt{X^2 + \epsilon_2 Y^2} \quad (44)$$

with $\epsilon_1 = \pm 1$ and $\epsilon_2 = \pm 1$

A non-normalized eigenvector corresponding to eigenvalue $\omega_{\epsilon_1,\epsilon_2}$ is then:

$$|\psi_{\epsilon_1,\epsilon_2}\rangle = \epsilon_1 a_{\epsilon_2}|a\rangle + \epsilon_1 c_{\epsilon_2}|c\rangle + |u\rangle + \epsilon_2|v\rangle \quad (45)$$

with:

$$a_\epsilon = S\sqrt{G + \frac{R}{2} + \epsilon\sqrt{S^2 + \frac{R^2}{4}}} \quad (46)$$

$$c_\epsilon = \left(\frac{R}{2} + \epsilon\sqrt{S^2 + \frac{R^2}{4}}\right)\sqrt{G + \frac{R}{2} + \epsilon\sqrt{S^2 + \frac{R^2}{4}}} \quad (47)$$

$$\begin{aligned} u = &\left(\Omega_{b1}S^* + \Omega^*_{c1}\tfrac{R}{2}\right)|b,1\rangle \\ &+ \left(\Omega_{b2}S^* + \Omega^*_{c2}\tfrac{R}{2}\right)|b,2\rangle \\ &\vdots \\ &+ \left(\Omega_{bn}S^* + \Omega^*_{cn}\tfrac{R}{2}\right)|b,n\rangle \end{aligned} \quad (48)$$

$$v = Y^2(\Omega^*_{c1}|b,1\rangle + \Omega^*_{c2}|b,2\rangle + \cdots + \Omega^*_{cn}|b,n\rangle) \quad (49)$$

Equation 45 can be reversed yielding, inter alia:

$$\begin{aligned} |a\rangle = \frac{1}{2(c_+a_- - c_-a_+)}&(-c_-|\psi_{++}\rangle \\ &+c_+|\psi_{+-}\rangle + c_-|\psi_{-+}\rangle - c_+|\psi_{--}\rangle) \end{aligned} \quad (50)$$

wherein indices +,− stand for +1, −1 respectively.

Solving the equation of motion for the eigenvectors yields:

$$|\psi_{\epsilon_1,\epsilon_2}(t)\rangle = e^{\frac{i}{2}\omega_{\epsilon_1,\epsilon_2}t}|\psi_{\epsilon_1,\epsilon_2}(0)\rangle \quad (51)$$

Now i consider a wave vector $|\phi(t)\rangle$ with $|\phi(0)\rangle = |a\rangle$. Its time dependency follows from equations 50 and 51:

$$\begin{aligned} |\phi(t)\rangle = \frac{1}{2(c_+a_- - c_-a_+)}&(-c_-|\psi_{++}\rangle e^{\frac{i}{2}\omega_{++}t} \\ &+ c_+|\psi_{+-}\rangle e^{\frac{i}{2}\omega_{+-}t} \\ &+ c_-|\psi_{-+}\rangle e^{\frac{i}{2}\omega_{-+}t} - c_+|\psi_{--}\rangle e^{\frac{i}{2}\omega_{--}t}) \end{aligned} \quad (52)$$

yielding:

$$\langle c|\phi(t)\rangle = \frac{c_-c_+}{(c_+a_- - c_-a_+)}(-\cos\frac{\omega_{++}t}{2} + \cos\frac{\omega_{+-}t}{2}) \quad (53)$$

Using equations 46 and 47 yields:

$$\langle c|\phi(t)\rangle = \frac{-S}{2\sqrt{S^2 + \frac{R^2}{4}}}(-\cos\frac{\omega_{++}t}{2} + \cos\frac{\omega_{+-}t}{2}) \quad (54)$$

yielding for the component on $|c\rangle$ of the wave vector $|\phi(t)\rangle$ at time t :

$$|\langle c|\phi(t)\rangle|^2 = W_{base}(\cos(\omega_+t) - \cos(\omega_-t))^2 \quad (55)$$

with:

$$\begin{aligned} \omega_\epsilon = \frac{\omega_{+,\epsilon}}{2} = \\ \frac{1}{2}\left[\frac{1}{2}\left(\sum_i|\Omega_{bi}|^2 + \sum_i|\Omega_{ci}|^2\right)\right. \\ \left.+\epsilon\sqrt{\left|\sum_i\Omega_{bi}\Omega^*_{ci}\right|^2 + \frac{1}{4}\left(\sum_i|\Omega_{bi}|^2 - \sum_i|\Omega_{ci}|^2\right)^2}\right]^{\frac{1}{2}} \end{aligned} \quad (56)$$

and:

$$W_{base} = \frac{\left|\sum_i\Omega_{bi}\Omega_{ci}\right|^2}{4\left|\sum_i\Omega_{bi}\Omega_{ci}\right|^2 + \left(\sum_i|\Omega_{bi}|^2 - \sum_i|\Omega_{ci}|^2\right)^2} \quad (57)$$

$|\langle c|\phi(t)\rangle|^2$ is the probability of the initial quantum state $|a\rangle$ to have evolved to $|c\rangle$ at time t, i.e. it is the probability of transition from the TCR-MHC well (a) to the intermediate well (c) via the TCR-pMHC well (b) between times 0 and t. Ignoring the time dependency, W_{base} is the (maximum) probability of this transition.

6.2 restriction to $\Omega_{bi} >> \Omega_{ci}$

I assume that generally the Ω_{bi} are substantially superior to the Ω_{ci} so that the equations have the simplified form:

$$W_{base} = \frac{\left|\sum_i\Omega_{bi}\Omega_{ci}\right|^2}{\left(\sum_i|\Omega_{bi}|^2\right)^2} \quad (58)$$

$$\omega_+ = \frac{1}{2}\sqrt{\sum_i|\Omega_{bi}|^2} \quad (59)$$

$$\omega_- = 0 \quad (60)$$

Equation 58 can also be written:

$$W_{base} = \frac{\sum_i|\Omega_{bi}|^2|\Omega_{ci}|^2}{\left(\sum_i|\Omega_{bi}|^2\right)^2} + \frac{\sum_{i\neq j}\Omega_{bi}\Omega^*_{bj}\Omega_{ci}\Omega^*_{cj}}{\left(\sum_i|\Omega_{bi}|^2\right)^2} \quad (61)$$

6.3 quantum measurement of well (c)

The evolution of the system from the intermediate state (c) may at best be described as a quantum measurement of the occupied/non-occupied status of quantum well (c). If quantum well (c) is occupied the antigen has been recognized and the process leading to destruction of the APC is started; otherwise the antigen has not been recognized and either an active process to undo the TCR-MHC and CD8 bounds is started or nothing happens. The opportunity window for making that measurement is a "recognition time" τ_{rec} corresponding to the contact time, possibly limited by active undoing of the TCR-MHC bound and of the CD8 bound. During τ_{rec} the smallest periodicity of

non-correlated measurements is $\frac{\pi}{\omega_+}$. So at the very best, i.e. if the quantum measurement of state (c) is fully optimized, the overall probability of an interaction leading to destruction of the APC following the initial event of formation of the CD8 bound and the TCR-MHC bound is:

$$W_{dest0} = \frac{\omega_+ \tau_{rec}}{\pi} W_{bind} \tag{62}$$

yielding:

$$W_{dest0} = \frac{\tau_{rec}}{2\pi} \left(\frac{\sum\limits_i |\Omega_{bi}|^2 |\Omega_{ci}|^2}{\left(\sum\limits_i |\Omega_{bi}|^2 \right)^{\frac{3}{2}}} + \frac{\sum\limits_{i \neq j} \Omega_{bi} \Omega_{bj}^* \Omega_{ci} \Omega_{cj}^*}{\left(\sum\limits_i |\Omega_{bi}|^2 \right)^{\frac{3}{2}}} \right) \tag{63}$$

6.4 Time averaging

Applying equation 8 to transitions between quantum wells (a) and (b) yields:

$$\Omega_{bi} = \frac{1}{\hbar} \mathbf{E}_{bi} \cdot (\mathbf{d}_b - \mathbf{d}_a) O_{bi;a} \tag{64}$$

wherein

$\mathbf{d}_b$ (resp $\mathbf{d}_c$) is the electric dipole moment in quantum well (b) (resp quantum well (a));

$O_{bi;a}$ is the overlap between the quantum states $|a\rangle$ and $|b,i\rangle$;

$\mathbf{E}_{bi}$ is the amplitude of the electric field on the frequency $\frac{1}{h}(\mathscr{E}_{bi} - \mathscr{E}_a)$ corresponding to the transition between states $|a\rangle$ and $|b,i\rangle$, with $\mathscr{E}_{bi}$ (resp $\mathscr{E}_a$ being the energy of quantum state $|b,i\rangle$ (resp $|a\rangle$).

Similarly, applying equation 8 to transitions between quantum wells (c) and (b) yields:

$$\Omega_{ci} = \frac{1}{\hbar} \mathbf{E}_{ci} \cdot (\mathbf{d}_b - \mathbf{d}_c) O_{bi;c} \tag{65}$$

I assume that the artificial electromagnetic wave does not cause transitions to state (c), so that the transitions from well (b) to well (c) are thermally stimulated only. The fields $\mathbf{E}_{ci}$ are therefore thermal only. I further assume that the frequency shift Δ_b between adjacent quantum states in well (b) is higher than the Rabi frequency of the thermally stimulated transitions from well (b) to well (c), so that the $\mathbf{E}_{ci}$ are mutually independent. Thus the Ω_{ci} are mutually independent and in particular they have mutually independent random phases, which are also independent from the phases of the Ω_{bi} . Time-averaging of the right member of equation 63 yields averaging on all possible phases of Ω_{ci} and therefore results in full cancellation of this right member.

The component of the electric field $\mathbf{E}_{ci}$ (resp $\mathbf{E}_{bi}$) along the direction of $\mathbf{d}_b - \mathbf{d}_a$ (resp $\mathbf{d}_b - \mathbf{d}_c$)can also be assumed to have a gaussian distribution. This is true for the thermal electric field but it is also a good approximation of the electric field of an artificial electromagnetic wave like terrestrial Digital Video Broadcasting (DVB-T). This results in the corresponding Ω_{ci} and Ω_{bi} having also a Gaussian distribution. Time-averaging of the Ω_{ci} separately in the numerator and denominator of the left member of equation 63 yields averaging on all possible values of the electric field and thus to the replacement of the Ω_{ci} and Ω_{bi} by their RMS values Ω_{ciR} and Ω_{biR}. Although this separate averaging of the numerator and denominator may not yield an exact value of the average of W_{dest0} it will be used as a reasonable approximation W_{dest1} of the time-averaged value of W_{dest0}, yielding the following equation:

$$W_{dest1} = \frac{\tau_{rec}}{2\pi} \left(\frac{\sum\limits_i \Omega_{biR}^2 \Omega_{ciR}^2}{\left(\sum\limits_i \Omega_{biR}^2 \right)^{\frac{3}{2}}} \right) \tag{66}$$

6.5 Position of well (c)

Once the biological system - including at least the TCR-pMHC system - is in well (c), it is assumed that a number of further steps (hereafter: the effector sequence) will necessarily follow which are expected to yield to destruction of the APC (in case the T cell is an effector T cell). This complex sequence of steps will occur much more easily if it can follow a descending energy line. It will then be a sequence of energy minimization steps likely to produce a predictable result, i.e. once the (c) state is entered the probability of destruction of the APC is near to 1.

For the effector sequence to follow a descending energy line, it must start from a high energy initial state. This initial state being being quantum well (c), it is expected that the energy of the occupied levels (inter alia the fundamental level) in quantum well (c) is higher than the energy of the occupied states in quantum wells (a) and (b).

The position of quantum well (c) is thus expected to be as shown on figure 7. Since it is substantially higher than all quantum states of interest in well (b), the overall bandwidth $\Delta_{bth} + \Delta_{cth}$ of the (b) to (c) transitions is relatively small as compared to the frequency of the transition. Ω_{ciR} is frequency-dependant but on this relatively small bandwidth it can be considered as constant. I therefore use $\Omega_{ciR} = \Omega_{cth}$ with Ω_{cth} a constant.

Equation 66 becomes:

$$W_{dest1} = \frac{\tau_{rec}}{2\pi} \frac{\Omega_{cth}^2}{\sqrt{\sum\limits_i \Omega_{biR}^2}} \tag{67}$$

6.6 plurality of quantum states in well (c)

There may be many quantum states in well (c) as shown on figure 7. When the power of the artificial wave is strong enough and the probability of occupation of well (c) is small, transitions to these states do not appreciably modify the amplitudes for the quantum states in well (b). Therefore the probability of the system being in quantum well (c) is the sum of W_{art} over all quantum states in well (c). I neglect transitions implying transition frequencies larger than $\frac{\Omega_{cth}}{2\pi}$. If the quantum states form a near continuum, the probability of the system being in quantum well (c) is summed on the number of slots having a bandwidth $\frac{\Omega_{cth}}{2\pi}$ within an overall bandwidth Δ_{cth} which, like Δ_{bth}, is less than 60 GHz. Following this summation, the overall transition probability to quantum well (c) becomes:

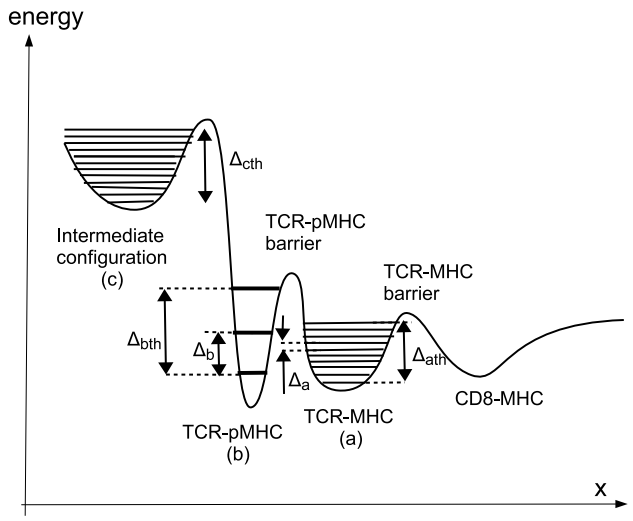

Figure 7: Energy profile along a minimum energy line of the interaction of a T cell with an APC, showing quantum energy levels in each well including a plurality of quantum states $|c\rangle$ in well (c), and a realistic position of quantum well (c)

$$W_{dest2} = \frac{2\pi\Delta_{cth}}{\Omega_{cth}} W_{dest1} \tag{68}$$

6.7 plurality of quantum states in well (a)

There are many quantum states $|a_j\rangle$ in well (a). Each of these quantum states has a probability of occupation $\mathscr{P}(j)$. The probability of destruction W_{dest1} must be calculated for each quantum state and weighted over these quantum states so that the probability of destruction is:

$$W_{dest} = \tau_{rec}\Delta_{cth}\Omega_{cth} \sum_j \frac{\mathscr{P}(j)}{\sqrt{\sum_i \Omega_{bij}^2}} \tag{69}$$

wherein Ω_{bij} is the RMS Rabi frequency corresponding to the transition from state $|a_j\rangle$ to state $|b,i\rangle$, which is stimulated either thermally or by the artificial electromagnetic wave.

6.8 calculation of Ω_{bij} for transitions stimulated by a simple artificial electromagnetic wave

f_{ij} is the transition frequency from state $|a_j\rangle$ to state $|b,i\rangle$ with $f_{ij} > 0$ if the transition is by photon absorption and $f_{ij} < 0$ if the transition is by photon emission. Here I assume that the artificial wave has a substantially constant power P_{art} per unit area over a bandwidth Δ_{art} comprising the transition frequency $|f_{ij}|$. I also assume that Δ_{art} is relatively small as compared to $|f_{ij}|$ so that the RMS Rabi frequencies Ω_{bij} of the transitions stimulated by the artificial wave can be considered as constant, and the RMS Rabi frequencies of the same transitions when thermally stimulated can also be considered as equal to a constant value Ω_{bth}. For the calculation of a generic $|\Omega_{bij}|$ two cases must be considered depending on whether or not the bandwidth is higher than the Rabi integration bandwidth $\delta\omega = 2\Omega_{bij}$ implied in causing stimulated transitions, as defined in equation 13.

- case 1: the bandwidth of the artificial wave is above the Rabi integration bandwidth of the transitions stimulated by it ($2|\Omega_{bij}| < 2\pi\Delta_{art}$)

In this case equation 18 yields:

$$\Omega_{bij} = 2c\mu_0 \frac{D_{ab}^2 (P_{art} + P_{thA})}{\hbar^2 2\pi\Delta_{art}} \tag{70}$$

wherein P_{thA} is the thermal power per unit area within the bandwidth of the artificial wave and is defined in agreement with equation 15 by :

$$P_{thA} = 2\pi\Delta_{art} kT \frac{f_{ij}^2}{c^2} \tag{71}$$

Equation 17 yields :

$$\Omega_{bth} = \frac{2}{(2\pi)^2} c\mu_0 kT \left(\frac{2\pi f_{ij} D_{ab}}{\hbar c}\right)^2 \tag{72}$$

combining equations 71, 70, 72 yields:

$$\Omega_{bij} = \left(\frac{P_{art}}{P_{thA}} + 1\right) \Omega_{bth} \tag{73}$$

- case 2: the bandwidth of the artificial wave is below the Rabi integration bandwidth of the transitions which it stimulates ($2|\Omega_{bij}| > 2\pi\Delta_{art}$)

In this case the Rabi frequency is calculated as if the wave was single mode:

$$\Omega_{bij} = \frac{D_{ab}}{\hbar} \sqrt{c\mu_0 (P_{art} + P_{thA})} \tag{74}$$

Combining equations 74 and the still valid equation 72 yields:

$$\Omega_{bij} = \Omega_{bth} \sqrt{\frac{2\pi\Delta_{art}}{2\Omega_{bth}}} \sqrt{\frac{P_{art}}{P_{thA}} + 1} \tag{75}$$

transition between cases 1 and 2: The transition between case 1 and case 2 happens when $2|\Omega_{bij}| = 2\pi\Delta_{art}$. The transition takes place for a power $P_{art} = P_{trans}$ of the artificial wave. P_{trans} can be calculated by equaling equations 73 and 75:

$$P_{trans} = \left(\frac{2\pi\Delta_{art}}{2\Omega_{bth}} - 1\right) P_{thA} \tag{76}$$

6.9 approximate values

I will use in this or the next sections some values shown on figure 7:

- the bandwidth Δ_{bth} (resp Δ_{ath}, Δ_{cth}) corresponding to the frequency shift between the fundamental state of well (b) (resp (a), (c)) and the highest energy quantum state which is localized in well (b) (resp (a), (c)).

- the frequency shift Δ_b (resp Δ_a) between adjacent quantum states in well (b) (resp (a)). This frequency shift is assumed to be constant, which amounts to assuming

that the quantum wells are harmonic. This approximation is valid at the bottom of the quantum wells but is much less valid in the upper part of the quantum wells.

I also assume that the RMS thermal Rabi transition frequency is constant for all transitions between quantum wells (a) and (b), with the value Ω_{bth}. This is quite a rough approximation in general, but when there is a frequency shift between occupied states of wells (a) and (b) which is sufficiently higher than $\Delta_{bth} + \Delta_{ath}$, the approximation becomes much better.

Equation 59 can be rewritten, assuming the energies of quantum states are equally spaced as happens in a harmonic quantum well:

$$\omega_+ = \frac{1}{2}\sqrt{\sum_{i=0}^{i=\frac{\Delta_{bth}}{\Delta_b}} \Omega_{bi}^2} \tag{77}$$

In strictly thermal conditions, equation 77 yields :

$$\omega_+ = \frac{1}{2}\sqrt{\frac{\Delta_{bth}}{\Delta_b}\Omega_{bth}^2} \tag{78}$$

In purely thermal conditions ω_+ defines the natural speed of the reaction with $\omega_+ = \frac{2\pi}{4\tau_{bind}}$, wherein τ_{bind} is a typical binding speed. This definition of τ_{bind} combined with equation 78 yields:

$$\Omega_{bth} = \frac{\pi}{\tau_{bind}}\sqrt{\frac{\Delta_b}{\Delta_{bth}}} \tag{79}$$

I also define a constant coefficient $\alpha < 1$ so that $\Omega_{cth} = \alpha\Omega_{bth}$

$$\Omega_{cth} = \alpha\frac{\pi}{\tau_{bind}}\sqrt{\frac{\Delta_b}{\Delta_{bth}}} \tag{80}$$

I now use a central value Ω_{bart} of Ω_{bij} corresponding to the center frequency $|f_{ij}| = F_{art} = \frac{1}{2}(F_{min} + F_{max})$. The following expressions of Ω_{bart} will be useful:

- case 1: combining equation 73 and 79 yields:

$$\Omega_{bart} = \frac{\pi}{\tau_{bind}}\sqrt{\frac{\Delta_b}{\Delta_{bth}}}\left(\frac{P_{art}}{P_{thA}} + 1\right) \tag{81}$$

case 2: combining equation 75 and 79 yields:

$$\Omega_{bart} = \pi\left(\frac{\Delta_b}{\Delta_{bth}}\right)^{\frac{1}{4}}\sqrt{\frac{\Delta_{art}}{\tau_{bind}}}\sqrt{\frac{P_{art}}{P_{thA}} + 1} \tag{82}$$

and combining equations 76 with equation 79 yields:

$$P_{trans} = (\Delta_{art}\tau_{bind}\sqrt{\frac{\Delta_{bth}}{\Delta_b}} - 1)P_{thA} \tag{83}$$

In these equations the thermal power is calculated by equation 71:

$$P_{thA} = 2\pi kT\frac{F_{art}^2}{c^2}\Delta_{art} \tag{84}$$

6.10 basis for the frequency and bandwidth condition

If any quantum states in quantum well (a) cannot make a transition stimulated by the artificial wave to quantum well (b), a TCR-pMHC which is in that quantum state is un-affected by the artificial wave. Assuming equal probabilities of occupation for all occupied quantum states in well (a) the overall W_{dest} can be written:

$$W_{ov} = \frac{N_{af}W_{dest} + N_{naf}}{N_{af} + N_{naf}} \tag{85}$$

wherein N_{af} is the number of affected quantum states and N_{naf} is the number of non-affected quantum states. The W_{dest} drops fast with increasing power of the artificial electromagnetic wave and typically reaches values in the order of less than 1/1000 as shown in Table 1. Therefore if only 1/100 of the quantum states in well (a) are non-affected, the overall W_{ov} is essentially equal to the proportion of non-affected quantum states in well (a) and is much higher than W_{dest}. A reasonable approximation of this situation is that all quantum states in well (a) must be able to make a transition to well (b) for W_{ov} to be affected at all. This will yield conclusions that exaggerate the brutality of the transition, but are otherwise reasonable.

This condition can be further split in two parts:

First I will examine whether each state in well (a) can make a transition to any "virtual" state in well (b) which has an energy comprised between the minimum and maximum energy in well (b). This amounts to ignoring the effect of the shift Δ_b between quantum states in well (b). This will yield a frequency condition.

Second I will admit that the frequency condition is respected and I will examine whether each state in well (a) can make a transition to a state in well (b) which energy is one of the quantized energies in well (b). This will yield a bandwidth condition.

The bandwidth and frequency conditions together express the more global condition that each occupied quantum state in quantum well (a) must be able to make a transition to quantum well (b).

6.11 Frequency condition

I use the following notations:

F_{fund} is the frequency of the transition between the fundamental state of quantum well (a) and the fundamental state of quantum well (b), i.e. $F_{fund} = \frac{1}{h}(\mathscr{E}_b - \mathscr{E}_a)$ where $\mathscr{E}_a$ (resp.$\mathscr{E}_b$) is the energy of the fundamental state of quantum well (a) (resp. quantum well (b)).

Δ_a (shown on figure 7) is the energy shift between quantum states in well (a), divided by Planck's constant h.

$\mathscr{P}(j)$ is assumed to be constant between $j = 0$ and $j = \frac{\Delta_{ath}}{\Delta_a}$ and zero outside this interval so that Δ_{ath} is the frequency shift (energy shift divided by h) between the highest energy occupied state in well (a) and the fundamental state in well (a).

The artificial wave is also assumed to have a constant spectral power $\mathscr{S} = \frac{P_{art}}{\Delta_{art}}$ over a single bandwidth extending from F_{min} to $F_{max} = F_{min} + \Delta_{art}$. I neglect the

increase of the frequency range due to the Rabi frequency, for the moment.

I consider a state $|a_j\rangle$ having a frequency shift $f_j = j\Delta_a$ with the fundamental state in well (a) with $F_{fund} - f_j > 0$.

$F_{fund} - f_j$ is the frequency shift between state $|a_j\rangle$ and the fundamental state of well (b). Frequency shifts between $|a_j\rangle$ and other states in well (b) are all higher than $F_{fund} - f_j$. Therefore, for the state $|a_j\rangle$ to be able to make a transition to any state of well (b), the artificial electromagnetic wave must comprise frequencies higher than $F_{fund} - f_j$. This implies the condition $F_{max} > F_{fund} - f_j$.

$F_{fund} - f_j + \Delta_{bth}$ is is the frequency shift between state $|a_j\rangle$ and the maximum energy state of well (b). Frequency shifts between $|a_j\rangle$ and other states in well (b) are all lower than $F_{fund} - f_j + \Delta_{bth}$. Therefore, for the state $|a_j\rangle$ to be able to make a transition to any state of well (b), the artificial electromagnetic wave must comprise frequencies lower than $F_{fund} - f_j + \Delta_{bth}$. This implies the condition $F_{min} < F_{fund} - f_j + \Delta_{bth}$.

Similar reasoning for the case $F_{fund} - f_j < 0$ yields $F_{max} > -(F_{fund} - f_j)$ and $F_{min} < -(F_{fund} - f_j) + \Delta_{bth}$ so the conditions can be generally expressed as:

$$F_{min} - \Delta_{bth} < |F_{fund} - f_j| < F_{max} \tag{86}$$

Since this condition must be verified by each f_i within the interval $[0, \Delta_{ath}]$ it results that the following frequency conditions must be respected:

$$F_{min} < \Delta_{bth} + \min_{0 \le f \le \Delta_{ath}} |F_{fund} - f| \tag{87}$$

$$F_{max} > \max_{0 \le f \le \Delta_{ath}} |F_{fund} - f| \tag{88}$$

These equations are altered when the Rabi integration bandwidth $\frac{2}{2\pi}\Omega_{bart}$ (i.e. twice the Rabi frequency) becomes higher than the bandwidth Δ_{art} (case 2) and generally when it cannot be neglected, because the artificial wave can then affect transitions which frequency is outside its frequency spectrum. The bandwidth of the artificial electromagnetic wave can be considered as enlarged by half the Rabi integration bandwidth on each end. The corresponding correction of the maximum and minimum frequencies yields:

$$F_{min} - \frac{1}{2\pi}\Omega_{bart} < \Delta_{bth} + \min_{0 \le f \le \Delta_{ath}} |F_{fund} - f| \tag{89}$$

$$F_{max} + \frac{1}{2\pi}\Omega_{bart} > \max_{0 \le f \le \Delta_{ath}} |F_{fund} - f| \tag{90}$$

6.12 bandwidth condition

In addition to the above frequency conditions it is necessary to take into account the fact that the quantum states in well (b) are separated by a frequency shift Δ_b .

If the bandwidth Δ_{art} is less than a bandwidth limit Δ_{lim}, some of the quantum states in well (a) will not be able to make a transition to well (b). The corresponding bandwidth limit (neglecting the increase of the bandwidth range due to the Rabi frequency for the moment) depends on the circumstances:

- if all transitions are by photon absorption, i.e. the occupied states in well (a) have significantly lower energies than the quantum states in well (b), then the states in well (b) to which a quantum state in well (a) can make a transition are all within a bandwidth Δ_{art}. If this bandwidth is less than Δ_b then for certain states in well (a) the states that can be reached in well (b) will be entirely comprised between two adjacent quantum states of well (b) separated by a frequency shift Δ_b. Since there is no quantum state in well (b) between these adjacent quantum states, no transition will be possible. Thus in this case $\Delta_{lim} = \Delta_b$.

- if all transitions are by photon emission the bandwidth limit is unmodified.

- if transitions can be both by photon emission and by photon absorption, i.e. quantum states in well (b) can have energies which are both higher and lower than quantum states in well (a), the bandwidth limit may decrease down to $\Delta_{lim} = \frac{\Delta_b}{2}$ depending on further parameters including F_{fund}.

Intermediate situations yield intermediate values of the bandwidth limit. For simplicity I will generally assume $\Delta_{lim} = \Delta_b$.

In case the Rabi integration bandwidth cannot be neglected, the bandwidth of the artificial wave can be considered as increased by half the Rabi integration bandwidth (i.e. one Rabi frequency) on each side, i.e. it is globally increased by one Rabi integration bandwidth. The bandwidth condition thus becomes:

$$\Delta_{art} + \frac{2}{2\pi}\Omega_{bart} \ge \Delta_{lim} \tag{91}$$

6.13 Approximated destruction probability

Here I assume that the frequency and bandwidth conditions are respected.

- in case 1 ($P_{art} < P_{trans}$) , the Rabi frequency of the transitions is Ω_{bart} over a bandwidth Δ_{art} and Ω_{bth} for the other transition frequencies so that:

$$\sum_{i=0}^{i=\frac{\Delta_{bth}}{\Delta_b}} \Omega_{bij}^2 \simeq \frac{\Delta_{art}}{\Delta_b}\Omega_{bart}^2 + \frac{\Delta_{bth} - \Delta_{art}}{\Delta_b}\Omega_{bth}^2 \tag{92}$$

by combining equations 69, 79, 81 and 92 the following is obtained:

$$W_{dest} = \frac{\tau_{rec}\Delta_{cth}\alpha\sqrt{\frac{\Delta_b}{\Delta_{art}}}}{\frac{P_{art}}{P_{thA}} + 1} \frac{1}{\sqrt{1 + \frac{\frac{\Delta_{bth}}{\Delta_{art}} - 1}{\left(\frac{P_{art}}{P_{thA}} + 1\right)^2}}} \tag{93}$$

- in case 2 ($P_{art} > P_{trans}$), the Rabi frequency of the transitions is Ω_{bart} over a Rabi integration bandwidth $\frac{2}{2\pi}\Omega_{bart}$ extending further than Δ_{art}, and Ω_{bth} for the other transition frequencies so that:

$$\sum_{i=0}^{i=\frac{\Delta_{bth}}{\Delta_b}} \Omega_{bij}^2 \simeq \frac{2\Omega_{bart}}{2\pi\Delta_b}\Omega_{bart}^2 + \frac{2\pi\Delta_{bth} - 2\Omega_{bart}}{2\pi\Delta_b}\Omega_{bth}^2 \tag{94}$$

In the above equation it was also assumed that $\Omega_{bart} < 2\pi\Delta_{bth}$ which is generally the case in practical applications (see Table 1). By combining equations 69, 79,82 and 94 , the following is obtained:

$$W_{dest} = \frac{\tau_{rec}\Delta_{cth}\alpha\tau_{bind}^{-\frac{1}{4}}\Delta_b^{\frac{5}{8}}\Delta_{bth}^{-\frac{1}{8}}\Delta_{art}^{-\frac{3}{4}}\left(\frac{P_{art}}{P_{thA}}+1\right)^{-\frac{3}{4}}}{\sqrt{1+\frac{\Delta_{bth}-\tau_{bind}^{-\frac{1}{2}}\Delta_b^{\frac{1}{4}}\Delta_{bth}^{-\frac{1}{4}}\Delta_{art}^{\frac{1}{2}}\left(\frac{P_{art}}{P_{thA}}+1\right)^{\frac{1}{2}}}{\tau_{bind}^{\frac{1}{2}}\Delta_b^{-\frac{3}{4}}\Delta_{bth}^{\frac{1}{4}}\Delta_{art}^{\frac{3}{2}}\left(\frac{P_{art}}{P_{thA}}+1\right)^{\frac{3}{2}}}}} \tag{95}$$

6.14 power threshold

The value of W_{dest} so calculated can reach a value superior to 1, which is not acceptable for a probability of destruction. When W_{dest} reaches a value of 1, it implies that the approximations made cease to be valid. But in a first approximation, the case of $W_{dest} = 1$ yields the limit value of power for which there is no appreciable degradation of the destruction probability, i.e. the power threshold. Since the value of W_{dest} is an upper bound, the power threshold which is obtained from it is an upper bound of the real power threshold.

The power threshold is obtained as follows:

- the value W_{trans} of W_{dest} for a power $P_{art} = P_{trans}$ is first obtained:

$$W_{trans} = \frac{1}{2}\alpha\frac{\tau_{rec}}{\tau_{bind}}\frac{\Delta_{cth}\Delta_b}{\Delta_{art}\sqrt{\Delta_{art}\Delta_{bth}}}\frac{1}{\sqrt{1+\frac{\frac{\Delta_{bth}}{\Delta_{art}}-1}{(2\Delta_{art}\tau_{bind})^2\frac{\Delta_{bth}}{\Delta_b}}}} \tag{96}$$

If $W_{trans} < 1$ the threshold value is determined by inversing formula 93:

$$P_{thres} = P_{thA}\left(-1+\sqrt{(\tau_{rec}\Delta_{cth}\alpha)^2\frac{\Delta_b}{\Delta_{art}}+1-\frac{\Delta_{bth}}{\Delta_{art}}}\right) \tag{97}$$

otherwise the threshold is obtained by inversing formula 95, which rarely happens as the power threshold is normally attained for powers lower than P_{trans}.

6.15 simplified analysis of the equations

In order to have a major effect on the destruction probability the artificial electromagnetic wave must verify:

- a bandwidth condition specified by equation 91 : its bandwidth - corrected for the Rabi integration bandwidth which is half the Rabi frequency- must be higher than a threshold. For low power values the correction can be ignored and there is a bandwidth threshold independent of power. For higher power values the correction must be taken into account so that the bandwidth threshold diminishes with power as a consequence of the increasing Rabi frequency.

- frequency conditions specified by equations 89 and 90: its center frequency -corrected for the Rabi integration bandwidth - must be within predetermined limits. For low power values the correction can be ignored and the predetermined frequency limits are independent of power. For higher power values the correction must be taken into account so that the frequency limits become more permissive.

- a power condition $P_{art} > P_{thres}$: its power must be superior to a threshold.

If these conditions are verified, the artificial wave affects the destruction probability in the manner described by equations 93 or 95 as the case may be.

	FM (single emitter)	FM (full band)	DVB-T (2 adjacent multiplexes)	GSM (fully loaded uplink and downlink)
center frequency (MHz)	100	100	600	900
bandwidth (MHz)	0.04	20	16	70
W_{dest} for P_{art}=1E-7W/m2	7.1E-03	7.1E-03	1.6E-01	7.4E-01
W_{dest} for P_{art} =1E-4W/m2	4.0E-05	4.0E-05	5.8E-04	1.1E-03
Power threshold	(1.1E-10)	4.9E-10	1.6E-08	7.4E-08
Pthres/PthA	(9.3E+05)	8.5E+03	9.5E+03	4.5E+03
"Rabi integration bandwidth" for 1E-7 W/m2 (MHz) *	41.59	41.59	3.00	0.31
"Rabi integration bandwidth" for 1E-4 W/m2 (MHz) *	1 315	1 315	219	146

Table 1: examples of numerical values. * the Rabi integration bandwidth is defined in section 3.2 and is twice the Rabi frequency.

6.16 orders of magnitude

It is possible to have a rough idea of the orders of magnitude implied by taking reasonable values of the parameters.

For calculation I take:

$\tau_{rec} = 0.03s$: This is half of the higher estimate for this parameter in [40].

$\tau_{bind} = 0.001s$: this is half the lowest estimate of τ_{rec} in [40]

$\Delta_{bth} = \Delta_{cth}$=4 GHz as a reasonable order of magnitude below 60 GHz taking into account that effects exist at least up to 2 GHz. This parameter has only a limited impact on the results.

$\alpha = 10^{-4}$: α has to be smaller than 1 but other than that there is no available knowledge about it. I have chosen this value so as to obtain a power threshold which is reasonably compatible with the powers at which cancers due to DVB-T have occurred.

Δ_b=10 MHz as this is a typical order of magnitude of the Δ_b which were affected where cancers occurred.

Exemplary calculation results are shown on table 1. For GSM the gap between uplink and downlink was ignored.

The numerical values in Table 1 should be considered very cautiously due to the uncertainties on all parameters and full lack of knowledge on parameter α, and it should also be taken into account that the results are upper bounds of W_{dest} and of the power thresholds. However

the results show that a reasonable choice of the parameters, compatible with existing knowledge, can also be compatible with the observed effects.

In interpreting these results, it is necessary to take into account the fact that W_{dest} is the probability of an interaction leading to destruction of the APC following the initial event of formation of the CD8 bound. Each T cell has many TCRs, so that more than one TCR may engage in a CD8 bound with a suitable pMHC of a target APC. Therefore, W_{dest} does not coincide with the probability of destruction of an APC by a T cell, or with the probability of the immune system overcoming a specific threat. These latter probabilities depend on the number of pMHCs presenting an abnormal peptide on each APC, on the number of APCs, and other parameters which were not discussed herein.

The power threshold shown for a single line FM emitter is the one calculated as per formula 97 corresponding to case 1 but does not apply to the specific case for two reasons. First, at 10^{-10} W/m2 for FM the calculated Rabi integration bandwidth is 1.37 MHz which is larger than the 0.04 MHz bandwidth of the single FM emitter, so that case 2 applies. Second, this Rabi integration bandwidth of 1.37 MHz at 10^{-10} W/m2 extends the 0.04 MHz FM bandwidth up to 1.41 MHz which is still lower than the 10 MHz Δ_b value, so that the bandwidth condition precludes any significant effect on the TCR-pMHC. So in this case the applicable power threshold of the effect on a TCR-pMHC is dictated by the bandwidth condition, not by the power condition.

The high Rabi integration bandwidth at 10^{-4} W/m2 for FM does not apply because the approximations made imply that the Rabi frequency is reasonably small compared to the carrier frequency of the artificial electromagnetic wave. However, it shows that the applicable "Rabi integration bandwidth" is large.

The case of a single FM emitter is little different from a CW exposure corresponding to $\Delta_{art} = 0$. When using cw exposure , case 2 always applies to the calculation of W_{dest} and Ω_{bart}. For sufficient power of a CW exposure the calculated W_{dest} is generally lower than 1 and the Rabi frequency can be high as is he case here for the single FM emitter, so that cw exposure can affect the TCR-pMHC systems, although with power thresholds resulting from the bandwidth condition which tend to be higher than the power thresholds calculated as per formula 97 for large bandwidth exposure.

6.17 structural characteristics of the TCR which may allow the interaction

Equation 72 combined with equation 17 yields:

$$D_{ab} = \frac{h}{f}\sqrt{\frac{1}{8\pi}\frac{c}{\mu_0 kT}\frac{1}{\tau_{bind}}\sqrt{\frac{\Delta_b}{\Delta_{bth}}}} \qquad (98)$$

Taking the same parameters as in section 6.16 for DVB yields $D_{ab} = 3.7 \cdot 10^{-25}$. Equation 9 applies with $O_{a;b} < 1$ so that the value of $|d_b - d_a|$ is larger than D_{ab}. On the other hand the dipole moment of the part of the TCR-pMHC which is outside the cell membrane is in the order of $3 \cdot 10^{-27}$ [3] [2]. Therefore $|d_b - d_a|$ is expected to be at least 100 times the dipole moment of the part of a TCR-pMHC which is outside the cell membrane of the T cell. This makes it unlikely that the electric dipole $|d_b - d_a|$ is realized only by that part of a TCR-pMHC.

The TCR is partly within the cell membrane and partly outside it. The part outside the membrane comprises about 4000 atoms. With an inter-atomic distance of 0.1 nm this yields an approximative diameter of 1.5 nm (which is probably under-evaluated). The thickness of the cell membrane is about 8 nm. The membrane potential is about -60 mV [46]. I consider the capacitor having a surface of 1.5x1.5 nm corresponding roughly to the surface of the cell's membrane which is occupied by the TCR, a thickness of 8 nm corresponding to the membrane thickness, a relative permittivity of 3 corresponding to a typical permittivity of lipids. This yields a capacitance of 5 pF. In view of the membrane voltage of 60 mV the electric charge carried by the capacitor is $3 \cdot 10^{-13}$ C. Multiplying this by the membrane thickness yields the dipole moment corresponding to the part of the cell membrane which is occupied by the TCR, yielding a dipole moment of $2.5 \cdot 10^{-21}$ C.m. This represents the dipole moment which would be induced in the TCR by the membrane potential if the surface density of ionic species on the inner and outer sides of the membrane was constant and if the TCR was able to directly conduct electrons between the parts of the TCR which are respectively inside and outside of the cellular membrane. As compared to this the real induced dipole moment in the TCR is increased because surface charges are not constant and decreased because it does not fully compensate surface charges, with an uncertain overall result. Therefore the above dipole moment of $2.5 \cdot 10^{-21}$ C.m. is a very rough order of magnitude of the dipole moment which can reasonably be induced in the TCR by the membrane potential.

Assuming a large overlap $O_{a;b} = 0.1$ with the above-calculated $D_{ab} = 3.7 \cdot 10^{-25}$, equation 9 yields $|d_b - d_a| = 3.7 \cdot 10^{-24}$. This is about 1000 times less than the above-mentioned value ($2.5 \cdot 10^{-21}$) of the induced dipole moment in a complete TCR. $|d_b - d_a|$ thus represents a relative difference of 1/1000th between the respective polarizabilities of the TCRs in configurations (a) and (b). Such difference is a very reasonable value.

Therefore, the electric dipole moment in the TCR is expected to be dominantly induced by the membrane potential. The electric dipole moment variation $|d_b - d_a|$ between configurations (a) and (b) is most likely provided by a difference of polarizability between configurations (a) and (b) which results in a corresponding difference in the induced dipole moment.

6.18 destruction probability for a general artificial wave in case 1

F_{fund} is the frequency of the artificial wave that can cause a transition from the fundamental state of well (a) to the fundamental state of well (b) with $F_{fund} > 0$ if the transition is by photon absorption and $F_{fund} < 0$ if the transition is by photon emission; Δ_a is the energy shift between quantum states in well (a), divided by Planck's constant

h.

I assume that the artificial wave has a frequency-dependent spectral power $\mathscr{S}(f)$ which is always below the transition spectral power $S_{trans}(f) = \left(\frac{2\pi\Delta_{art}}{\Omega_{bth}} - 1\right)(2\pi kT\frac{f^2}{c^2})$ calculated for a Δ_{art} which is the smallest bandwidth on which the artificial wave has a substantially constant spectral power. Typically for a multiplex of DVB waves I would use $\Delta_{art} = 8$ MHz. This condition is quite restrictive but the results obtained below are likely to have a wider application. Equation 69 yields:

$$W_{dest} = \tau_{rec}\Delta_{cth}\Omega_{cth}\sum_{j\geq 0}\frac{\mathscr{P}(j)}{\sqrt{\sum_{i=0}^{i=\frac{\Delta_{bth}}{\Delta_b}}\Omega_{bij}^2}} \tag{99}$$

with

$$\Omega_{bij} = \left(\mathscr{S}(|f_{ij}|)\frac{c^2}{2\pi kTf_{ij}^2} + 1\right)\Omega_{bth} \tag{100}$$

and

$$f_{ij} = F_{fund} + i\Delta_b - j\Delta_a \tag{101}$$

These equations can be summarized as:

$$W_{dest} = \tau_{rec}\Delta_{cth}\alpha \sum_{j\geq 0}\frac{\mathscr{P}(j)}{\sqrt{\sum_{i=0}^{i=\frac{\Delta_{bth}}{\Delta_b}}\left(\frac{c^2\mathscr{S}(|F_{fund}+i\Delta_b-j\Delta_a|)}{2\pi kT(F_{fund}+i\Delta_b-j\Delta_a)^2}+1\right)^2}} \tag{102}$$

Figures 8, 9, 10 shows W_{dest} as a function of Δ_b before and after adding DVB to the existing analog TV in Nantes, Paris and Thorens Glieres respectively. W_{dest} was computed using equation 102. Each DVB multiplex and each analog TV channel were modelled as 8MHz constant spectral power channels. FM radio when present was modelled as a full FM bandwidth having the same spectral power as the TV channels. F_{fund} =88 MHz. $\mathscr{P}(j)$ was a linearly decreasing function of j which was maximum at $j = 0$ and zero at $j = \frac{4\cdot 10^6}{\Delta_a}$ with $\Delta_a = 0.2\cdot 10^6$ Hz. Other parameters were as specified in section 6.16. Thorens-Glieres did never have a local FM emitter nor an analog TV emitter in the VHF bandwidth below 220 MHz, and this explains the major differences between the curve for Thorens Glieres and the other curves. Although the curves of Nantes and Paris share common features, the added attenuation zones do not correspond, for example in Nantes the destruction probability was attenuated for the Δ_b values of 42 to 48 MHz, whilst it is not the case in Paris. The different curves may explain different local reactions as a particular cancer may be best controlled by TCRs in a Δ_b zone which was attenuated in one place and not in another.

However there are strong uncertainties as to the applicability of these curves:

In the frequency domain, the FM bandwidth is not a flat signal but instead comprises a plurality of single FM signals having each a very small bandwidth, with a single-station exact spectrum which varies depending on what

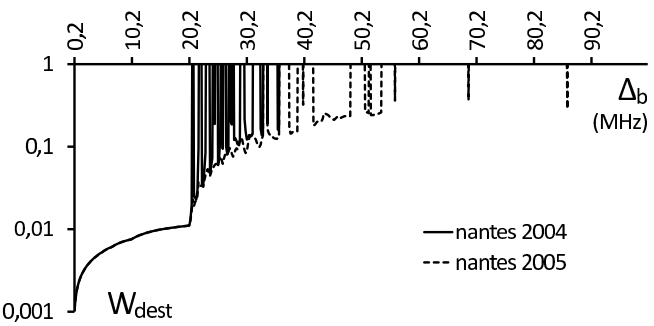

Figure 8: probability of destruction of an APC by a TCR as a function of the frequency shift Δ_b between consecutive quantum states in well (b), in Nantes prior to (2004) and after (2005) start-up of DVB

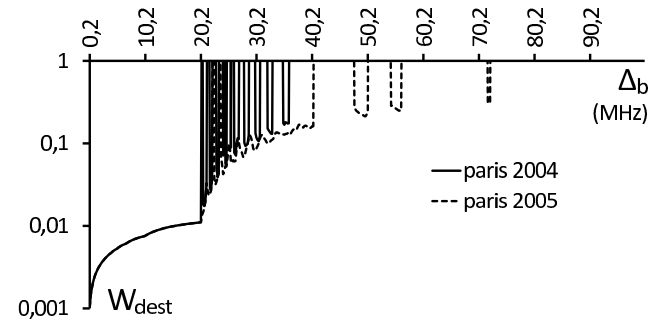

Figure 9: probability of destruction of an APC by a TCR as a function of the frequency shift Δ_b between consecutive quantum states in well (b), in Paris prior to (2004) and after (2005) start-up of DVB

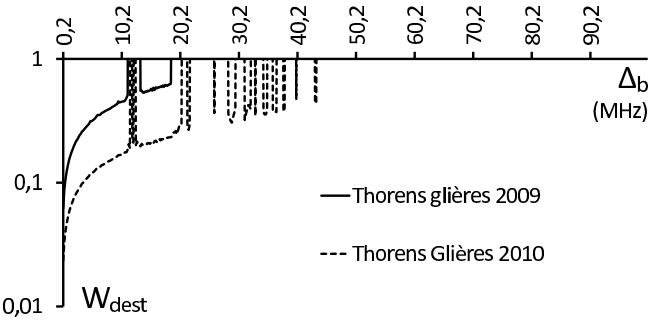

Figure 10: probability of destruction of an APC by a TCR as a function of the frequency shift Δ_b between consecutive quantum states in well (b), in Thorens-Glieres prior to (2009) and after (2010) start-up of DVB

is being broadcast. The individual FM signals are separated from each other by gaps in the order of 400 kHz. For evaluating the effects of these FM stations, the gaps can be ignored and the spectrum can be considered as flat if the Rabi integration bandwidth corresponding to a single station is superior to the gap. With the parameters used for Table 1, this occurs at a power of 1 nW/m2 of a single signal. Such level of power is very commonly exceeded, which justifies considering the FM band as relatively flat. However, with different parameters the result may differ. If the gap cannot be ignored, then in the 1 to 20 MHz Δ_b frequencies the spectrums shown for example on figure 8 would appear as comprising many un-attenuated "holes" in the case of an FM signal alone, with the DVB signals acting as "gap filler" and providing some level of attenuation in the holes without reaching the general attenuation of the FM band. This can have unexpected effects.

The analog TV signal has a varying signal power and spectrum, depending on what is being broadcast. This varying signal power and spectrum produces a marginal anti-cancer, pro-autoimmune effect as described in Table 2, column E. This marginal effect may partly compensate any transient effects on any Δ_b frequency for which the analog TV signal contributes to the attenuation of W_{dest}.

Unlike any other signal, the DVB signal has almost a perfectly constant flat spectrum when integrated even on a relatively short timescale, without variations in frequency. The transient effects of DVB are not attenuated by any marginal pro-autoimmune effect due to time variation of the signal. The present theory applies directly and almost ideally to DVB signals. DVB generally may be more pro-cancer than other signals, at equal power and bandwidth. But the effects of mixing DVB with other signals are uneasy to evaluate properly.

The GSM signal and other frequencies have also been ignored. This is justified only for T cells having a frequency condition which excludes the GSM. The interaction of time-varying signals like GSM with permanent signals like TV is discussed in section 8.

6.19 justification of the restriction to $\Omega_{bi} >> \Omega_{ci}$

This restriction is also embodied in the parameter α which is less than 1, i.e. $\Omega_{bth} > \Omega_{cth}$. This implies that the TCR binds best to the pMHC when Ω_{bth} is lowest, i.e. when it has the lesser tendency to move from quantum well (a) to quantum well (b). This is somewhat counter-intuitive as one would expect TCRs which go faster into quantum well (b) to also go faster into quantum well (c) and thus to best bind the pMHC, as would actually be the case with $\Omega_{bth} < \Omega_{cth}$.

This can be best understood using a 3D picture as shown on figure **??**. Quantum wells (a) and (b) are limited inter alia by a strong energy barrier and separated from each other by a weaker energy barrier ("passage"). The minimum energy path passes through the weaker energy barrier. In order to efficiently block passage between the two quantum wells, the peptide must have exactly the shape of the passage left by the stronger energy barriers, otherwise if the peptide "is too small" an alternate

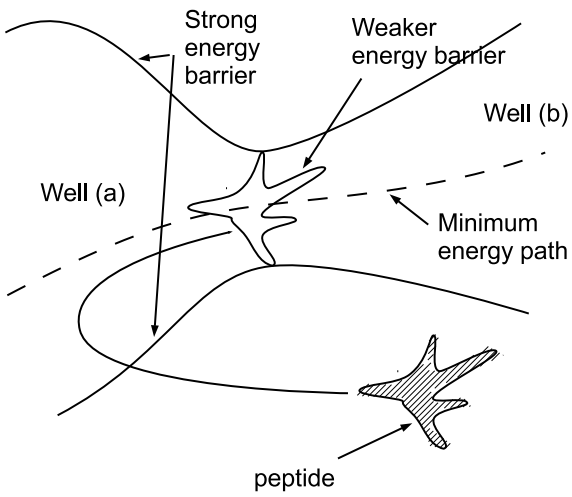

Figure 11: a 3D picture of a mechanism of peptide recognition.

minimum energy path can bypass it without crossing the strong energy barrier or if the peptide "is too large" it cannot fit in the passage so that there is also a minimum energy path through the passage which does not cross the strong energy barrier. When the peptide blocks the passage efficiently the barrier between quantum wells (a) and (b) becomes stronger and the Ω_{bth} is significantly reduced so the peptide is "recognized" and the system goes into non-represented well (c). So the mechanism makes it possible to differentiate even between similar peptides based on their capacity to block the passage between the quantum wells, which is determined by steric effects.

The reality is in many dimensions and is a lot more complex than that, but this simple picture helps in understanding that a mechanism based on blocking a minimum energy path (as is the case when $\Omega_{bth} > \Omega_{cth}$) may be a lot more specific than a mechanism based on accelerating transitions between two quantum wells (as would be the case with $\Omega_{bth} < \Omega_{cth}$). The capacity to accelerate a transfer from well (a) to well (b) relies essentially on electrostatic attraction, whilst the capacity to block an existing path relies essentially on steric effects. The capacity to block a path (under the hypothesis $\Omega_{bth} > \Omega_{cth}$) is like the capacity of a mechanical piece to block a flow of water in a conduit: the mechanical piece must have exactly the right shape. The capacity to accelerate a path (under the hypothesis $\Omega_{bth} < \Omega_{cth}$)is like the capacity of two magnets to attract each other. The blocking test is much more specific.

This simplistic argumentation is not a full justification but it helps in understanding why this specific binding principle, including the restriction $\Omega_{bth} > \Omega_{cth}$, is probably advantageous for living organisms (because it is more specific) and has been selected through evolution.

6.20 validity of the model

The qualitative fact that the artificial electromagnetic wave diminishes the destruction probability is readily apparent from formula 63 in view of the fact that the artificial electromagnetic wave increases the Rabi frequencies Ω_{bi}

but not the Rabi frequencies Ω_{ci}. It is thus independent of the approximations made in sections 6.5 and further. This essential qualitative conclusion thus depends only on fundamental features of the model.

The complete model of the TCR-pMHC interaction was developed using a number of simplifications. For example the fact that the quantum states in a quantum well are separated by a constant frequency shift Δ_b is valid for single dimensional quantum wells and is likely valid in many case at the bottom of a non-symmetrical quantum well, but generally a multiplicity of different frequency shifts exist in a multi-dimensional quantum well. The thermal Rabi frequency Ω_{bth} was considered constant on a predefined interval, whilst obviously the reality is more complex. The gaussian approximation for the electric field of the artificial electromagnetic wave is a good approximation for DVB-T but may not be an acceptable approximation for certain other artificial electromagnetic waves, like FM radio or analog TV. The present model thus does not reflect the full complexity of the reality. Therefore, effects which are not predicted by the model may appear, and inter alia, quantitative results predicted by the model may differ from reality.

The quantitative developments were however necessary to check that the orders of magnitude of the model's predictions are compatible with observed phenomena and to gather a reasonable understanding of the phenomena: fundamental bandwidth, frequency and power conditions for observing an effect of exposure on a TCR-pMHC system, and interaction between the effects of different artificial waves. Whilst these results should not be applied blindly, they are useful for understanding the dependency of biological effects on various parameters.

7 Reaction of the immune system to artificial electromagnetic waves

7.1 thymus selection in transient and permanent exposures

Increased exposure results in decrease in the destruction probability W_{dest} and therefore a pro-cancer, anti-auto-immune, pro-pathogen effect. Reversely, decreased exposure results in an anti-cancer, pro-auto-immune, anti-pathogen effect. However the selection criteria in the thymus is based on a fixed range of the W_{dest} relative to pMHC involving peptides of the self presented in the thymus. After the onset of a modified exposure condition, thymus selection and extra-thymic regulation processes (for example implying regulatory T cells) progressively modify the T cells to reinstate the original range of W_{dest} related to pMHCs involving peptides of the self. This effect of thymus selection impacts only marginally the destruction probability W_{dest} relative to pMHCs involving peptides of the non-self, because the selection criteria in the thymus is essentially independent of this destruction probability. Thus, the effects of a modified permanent exposure on autoimmune disease or cancer are essentially transient, whilst a permanent effect is expected on infectious diseases.

This interaction of thymus selection with electromagnetic waves can be better understood using figure 12. For any T cell I note W_{min} (resp. W_{max}) the minimum (resp. maximum) value of its destruction probability W_{dest} relative to pMHC complexes involving peptides of the self presented in the thymus. Positive selection in the thymus eliminates T cells which do not bind sufficiently to any pMHC presented in the thymus and therefore select T cells having a W_{min} superior to a threshold. Negative selection eliminates T cells which bind too strongly to any pMHC presented in the thymus and therefore selects T cells having a W_{max} lower than a threshold. Figure 12(A) shows the T cells positioned in a $\log W_{max}, \log W_{min}$ diagram. Areas where the T cells are eliminated by positive or negative selection are dashed. The selected area comprising those T cells which survive both positive and negative selection is shown. Figure 12(C) shows how this is modified by a change of exposure from low to high. All T cells have their W_{dest} diminished, resulting in the existing T cells moving down and left on the diagram. This results in an immediate pro-cancer, anti-auto-immune, pro pathogen effect. Figure 12(B) shows how thymus selection and extra-thymic regulation processes progressively modify this situation. Newly selected T cells fill the part of the originally Selected Area which was emptied by the change from low to high exposure. T cells that were brought out of the Selected Area by the change from low to high exposure progressively undergo apoptosis outside of the thymus [44]. Remaining T cells which W_{min}, W_{max} was modified but remained in the Selected Area are unaffected by the change. So after full stabilization the diagram looks exactly like figure 12(A). The newly selected T cells bind more strongly to self pMHCs than the newly eliminated T cells. The cells which are on the right border of the Selected Area have exactly the same W_{max} in the permanent high exposure situation as in the permanent low exposure situation. Since these cells are most implied in the control of cancer this essentially results in a reinstated autoimmune/cancer balance.

The newly selected T cells are however not selected for improved binding to the non-self. Although the initial pre-exposure situation is reinstated relative to the self, it is not reinstated relative to the nonself. Therefore in the permanent high exposure case there is a net pro-pathogen effect.

Figure 12(D) shows how the diagram is modified by a transition from high to low exposure. The existing T cells have increased W_{dest} relative to pMHCs of the self yielding to an anti-cancer, pro-autoimmune, anti-pathogen effect. This situation is then modified by thymic selection and extra-thymic regulation mechanisms again restoring the appearance of figure 12(A).

Figure 12 shows only two dimensions corresponding to the variables W_{min} and W_{max}. Other dimensions which are of importance are Δ_b and any lower and upper frequency limits as per section 6.11. For the discussion I will ignore the upper and lower frequency limits and concentrate on Δ_b. T cells which form TCR-pMHC bounds with the self having a Δ_b outside the Δ_b range affected by the

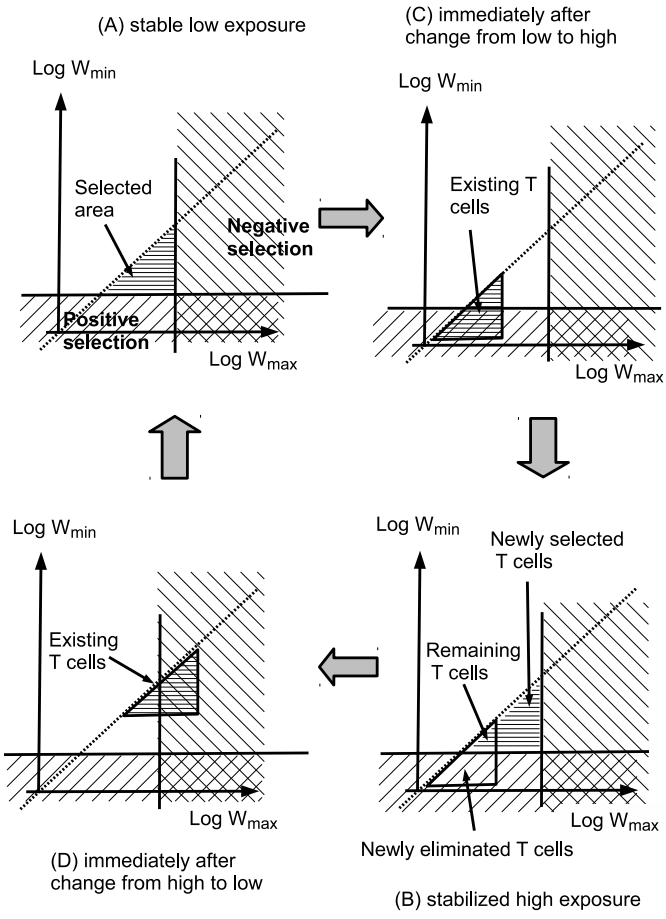

Figure 12: selection of T cells by the thymus in permanent or transient low or high exposure situations.

artificial waves are un-affected by exposure and any such T cells which were selected by the thymus in un-exposed conditions will still be selected in exposed conditions. After the onset of high exposure conditions, a line of T cells which lost control of a cancer may be replaced by a line of T cells in a non-affected Δ_b range which will control the cancer. However as discussed in section 7.3 such T cell line is generally expected to be a recent thymus emigrant so that this circumstance does not affect the existence of a transient pro-cancer period lasting until the thymus produces a new T cell line able to control the cancer. In all cases the duration of the transient period (with respect to cancer) is linked to thymus output.

Whilst exposure affects thymus selection, it is not expected to affect production of T cell precursors in the bone marrow. Depending on the power of the artificial wave, the proportion of the T cells within the affected Δ_b range which are capable of surviving positive and negative thymus selection varies. Negative thymus selection is known to eliminate more T cells than positive thymus selection so for a moderate power of the artificial wave (relative to thermal power) the number of T cells surviving thymus selection in exposed conditions may increase. But if exposure is strong, there may not be any T cell precursor amongst those having a Δ_b affected by exposure which is capable of surviving positive selection in the thymus. In this case thymus selection under exposed conditions simply results in the elimination of all T cells forming TCR-pMHC bounds with the self which are within the affected Δ_b range. Such T cells are also eliminated extra-thymically by apoptosis. Therefore under strongly exposed conditions the population of mature T cells shifts towards higher Δ_b values and the number of T cells surviving thymus selection diminishes.

When this shift occurs new thymus-selected cells in a non-affected Δ_b range replace eliminated T cells in the long term, cancelling the transitional pro-cancer, anti-auto-immune effect, and in this respect the shift may not fundamentally modify the apparent behaviour of the immune system during a transition. The elimination of a Δ_b range may result in a diminished anti-cancer capability of the immune system in permanent exposure conditions, but only if a significant number of cancers are both controllable by T cells forming TCR-pMHC bounds within the affected Δ_b range and not controllable by T cells forming bounds outside that range. There is no experimental evidence that this occurs in practical cases (see section 9) so this possibility will be ignored.

7.2 thymus selection in alternating high/low exposure

Figure 13 shows how the situation is modified in a case of alternance between high exposure and low exposure conditions. Existing T cells populate:

- a fully populated area which comprises T cells that verify the thymus selection conditions in both the high exposure and low exposure situation.

- partly populated area A [resp. B] comprising T cells which verify the thymus selection conditions in the low [resp. high] exposure situation (but may have been se-

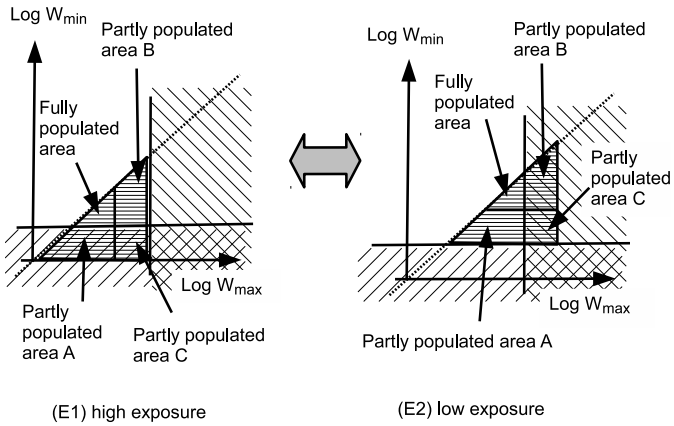

Figure 13: selection of T cells by the thymus in an alternating high/low exposure situation.

lected partly under high exposure conditions and partly under low exposure conditions).

- partly populated area C comprising T cells that have undergone part of their maturation under low exposure conditions and part of their maturation under high exposure conditions and which do not verify the thymus selection conditions in high exposure conditions nor in low exposure conditions.

In the high exposure conditions of figure 13 (E1) the T cells in partially populated areas A and C, having a W_{dest} lower than W_{min}, are essentially deprived of any destruction capabilities relative to pMHCs of the self. The T cells in partly populated area B have a normal destruction capability relative to self pMHCs although they are in smaller number. The global effect relative to the self is essentially dictated by the T cells in partially populated area B. There is a marginal pro-cancer effect due to the diminished number of these cells but there is no change in W_{dest}. There is no auto-immune effect.

The behavious towards the self is essentially dictated by the T cells on the right border of the area comprising T cells. In the low exposure conditions of figure 13 (E2) these T cells are in partially populated areas B and C and have higher than normal values of W_{dest}, thus creating a pro-autoimmune effect.

During the low exposure periods, T cells in partly populated areas B and C attack the self, creating irremediable auto-immune damage, and attack any cancer with increased strength. During the high exposure periods, there are no auto-immune effects but there is also no mechanism to repair the previously caused auto-immune damage, so there is a net time-integrated auto-immune effect. During the high exposure period, T cells behave essentially normally as if the exposure conditions were constant. Their smaller numbers in area B only has a marginal effect on cancer because as long as a single line of T cells efficient against a cancer can be found, the behaviour will be normal. The net time-integrated effect is thus anti-cancer.

The shift to higher Δ_b ranges affects alternative high/low exposure regime only marginally. Insofar as the duration of each high and low exposure period is sufficiently shorter than thymus transit times (which are in the order of several weeks), a T cell does not normally undergo all of its positive and negative selection steps under the same exposure level. If exposure level is sufficiently high to eliminate all T cells within an affected Δ_b range by positive selection, then only those T cells which have undergone their positive selection under high exposure conditions will be eliminated. Other T cells will survive positive selection, with abnormally aggressive T cells undergoing negative selection during high exposure periods surviving thymus selection and yielding the same anti-cancer, pro-auto-immune effects as if there had been no elimination by positive selection.

7.3 Extraction from T cell library in transient or permanent exposure

Naive mature T cells produced by the thymus are stored in peripheral lymphoid organs and a permanent T cell library is maintained in each individual even after thymus involution, through a combination of homeostatic turnover and an increase of naive T cell lifetime [45] . Therefore a line of T cells which becomes inefficient against a cancer or a pathogen following an increase in artificial electromagnetic waves can be replaced by another line of T cells in the existing naive T cell library of the affected individual, which is not necessarily a recent thymic emigrant, but may still be efficient in the presence of the artificial wave. Such replacement implies that a new primary reaction must take place and that a T cell line able to control the cancer or the pathogen for which control has been lost must exist in the existing T cell library.

T cells able to control a cancer tend to be near the negative selection limit in figure 12 so that immediately after a change from low to high exposure , corresponding to figure 12 (C), there is normally little or no existing T cell near the negative selection limit in the whole range of Δ_b values affected by the low to high transition, and therefore the immune system is generally unlikely to take back control of a cancer using T cells of the existing T cell library in that range of Δ_b values.

Even outside that range the population of naive T cells able to control cancer is reduced because such T cells tend to be aggressive against the self and therefore they are likely to have a shorter extra-thymic lifetime. Therefore, cancer control generally implies recent thymic emigrants rather than older T cells of the T cell library. This also explains why cancer occurs much more often after 45 years of age, i.e. after thymus involution.

For these reasons, new primary reactions implying newly thymus-selected T cells is most likely the dominant mechanism under which the immune system can control cancer after a change from low to high exposure, and cancer control is relatively little affected by new primary immune reactions making use of the pre-existing T cell library.

T cells able to control an infectious disease may be near the negative selection limit if the implied pathogen "mimics" the self, i.e. if its strategy for fooling the immune system is to have antigens that closely resemble those of the self. Immune control of such pathogens may also be dominantly using newly thymus-selected T cells. But T cells able to control an infectious disease that is not self-

mimicking are not particularly likely to be near the negative selection limit on figure 12 (C). They have a relatively low affinity for the self and therefore they are less likely to be eliminated extra-thymically and they may also have a longer life span. For these reasons a T cell line able to take back control of such infection is more likely to be found in the existing T cell library of an affected individual, without resorting to newly thymus-selected T cells.

Thus, following a low to high exposure transition for a pathogen which is not self-mimicking, a new T cell line may be found amongst the pre-existing T cells which can control the pathogen. Such T cell line may be chosen amongst T cells that have a Δ_b which is not affected by artificial waves, if T cells in that non-affected Δ_b range exist which can control the pathogen, yielding a shift of the activated T cell lines to higher Δ_b values. Such T cell line may also be found amongst T cells with an affected Δ_b value but this can be uneasy because such T cell lines have a diminished W_{dest} in high exposure conditions which is not compensated for by thymus selection. Thus, if pathogen control preferentially requires T cells within the affected Δ_b range, it is difficult to find a replacement T cell line and a net pro-pathogen effect occurs even in permanent regime. The duration of the transition period is the duration of the primary reaction under which a replacement T cell line can be activated. If a replacement T cell line can be found and the affected individual survives the transition period, his immune system may recover.

Therefore the effect of a low to high exposure transition on a pathogen which is not self-mimicking comprises:

(a) a transient effect corresponding to the immediate suppression of ongoing immune responses, yielding quick deaths when a new primary response cannot be found fast enough, and

(b) if pathogen control preferentially requires T cells within the affected Δ_b range, a long term effect, corresponding to the generally lengthened primary immune response and weakened affinity of T cells for the pathogen, which in the case of a pathogen which is not self-mimicking is not compensated for by thymus selection in the long term.

In the case of alternating high and low exposure for a pathogen that is not self-mimicking, the immune response is at worst stopped during the high exposure periods. The attacks against non-self are essentially postponed during the high-exposure periods. The effects on a specific pathogen depend on this pathogen's capacities to exploit a temporary absence of immune response and survive a temporary immune response.

7.4 weakening of inflammatory responses

Inflammatory responses to extrinsic agents are not in essence directed against the self. After a low to high transition the implied T cells may become inefficient and be later replaced by T cells from the existing T cell library. However the replacement T cells normally have a lower affinity in high exposure conditions to antigens of the extrinsic agents than the original T cells had under low exposure conditions, so that the inflammatory reaction is either suppressed (in the absence of a replacement) or at least weakened (if a replacement is possible). Therefore a low to high exposure transition results in both a transient effect when the inflammatory response ceases, and a long term effect because any renewed inflammatory response is weaker than the original one.

	A	B	C	D	E
Immune threat	Permanent low exposure (thermal)	Permanent high exposure	Transition from Low to High exposure: period immediately after transition	Transition from High to Low exposure : period immediately after transition	Alternance between low and high exposure (at least half time low exposure)
cancer	standard	Standard	Pro cancer	Anti cancer	Anti cancer
auto-immune disease	standard	standard	Anti auto-immune	Pro auto-immune	Pro auto-immune
Pathogen (not self-mimicking)	standard	Pro pathogen	Pro pathogen	standard	Pro Pathogen
Inflammatory response against non-self.	standard	Anti inflammation.	Anti inflammation.	standard	Anti-inflammation

Table 2: Table of effects of the electromagnetic waves.

7.5 reference table for effects of electromagnetic waves

The effects discussed in the preceding sections are summarized in Table 2. The effects shown on this table do not necessarily appear for all cancers or all pathogens: a cancer or a pathogen which is controlled by T cells forming TCR-pMHC bonds outside an affected Δ_b range will remain un-affected. A pathogen which is controlled by T cells forming bonds within an affected Δ_b range but which can also be controlled by T cells outside that range may be little affected in case of a permanent high exposure as per column B. When a pro-cancer or pro-pathogen effect exists it becomes detectable (through death rates) only when it is sufficiently strong to cause loss of control of the cancer or pathogen by existing T cell lines. Exceptions to the behaviours predicted by this table can also occur as discussed in section 8 for example.

In this table, the transient period immediately after a change from high to low exposure is standard (relative to standard low exposure conditions) but is anti-pathogen relative to the previously existing high exposure condition.

7.6 T cell selection after thymus involution

Thymus involution never really ends but around the age of 40 years it is generally recognized that there is a transition and for many purposes thymus involution may be considered as terminated. After this critical age, the production of new naive mature T cells is heavily diminished. However, production of naive mature T cells also occurs extra-thymically [35]. Also, thymus output was evidenced even in aged animals [25]. Both mechanisms contribute to the continued existence of processes of selection of new naive mature T cells post thymus involution. Therefore after thymus involution the transition periods of Table 2 columns C and D are longer but not "infinitely long".

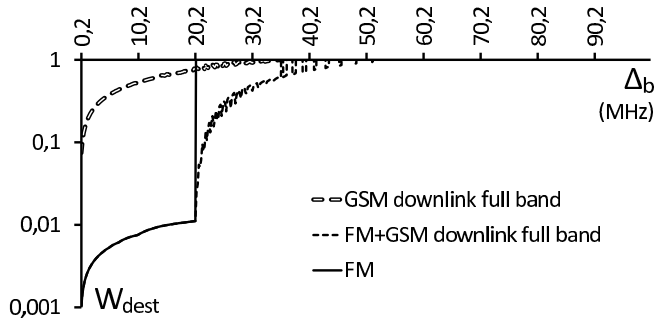

Figure 14: probability of destruction of an APC by a TCR as a function of the frequency shift Δ_b between consecutive quantum states in well (b), for various combinations of FM radio and GSM downlink. Average FM spectral power is equal to peak GSM spectral power

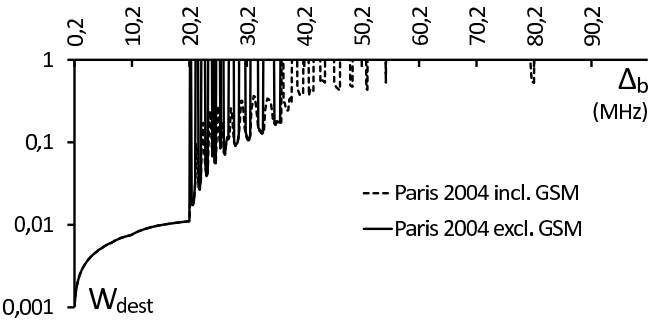

Figure 15: probability of destruction of an APC by a TCR as a function of the frequency shift Δ_b between consecutive quantum states in well (b), in Paris in 2004 including and excluding GSM.

8 interaction between permanent and time-varying artificial electromagnetic waves

Time-varying electromagnetic waves such as GSM are expected to generally have a permanent anti-cancer effect and permanent electromagnetic waves such as DVB are expected to generally have a transient pro-cancer effect. However interaction between these two sorts of waveforms can yield different results.

Figure 14 shows the attenuated W_{dest} as a function of Δ_b , calculated as in section 6.18, for different combinations of FM and GSM signals, at equal spectral power of the FM and GSM signals.

For GSM alone, corresponding to a full downlink bandwidth 925 to 960 MHz, the affected Δ_b values are generally below 30 MHz. For FM, corresponding to a full bandwidth 88 to 108 MHz, the affected Δ_b values are below 20 MHz. For FM and GSM together, the affected values go to roughly 35 MHz. When FM and GSM are present together with the FM spectral power being equal to the peak GSM spectral power, a TCR having a Δ_b in the range 0 to 20 MHz is not affected by the pro-autoimmune, anti-cancer effects of GSM, because the attenuation is the same with or without GSM (despite the fact that when GSM only is present it is affected). But, still when FM and GSM are present together, a TCR having a Δ_b in the range 20 to 35 MHz is affected by the pro-autoimmune, anti-cancer effects of GSM, because the attenuation is different with or without GSM. This includes the 30 to 35 MHz range which is virtually non-affected in the presence of GSM only. Also, in the Δ_b frequency range of 20 to 35 MHz the attenuation is much stronger when FM and GSM are present together than with GSM only. Therefore the presence of a full FM band considerably modifies the effect of GSM by causing the Δ_b values affected by GSM to shift towards higher frequency and increasing the difference between attenuated W_{dest} with or without GSM power being "on", which also increases the pro-auto-immune, anti-cancer effect of GSM on any TCRs having the corresponding Δ_b (above 20 MHz in the instant case).

This modification of GSM effects by permanent electromagnetic waves also exists for digital and analog TV. In

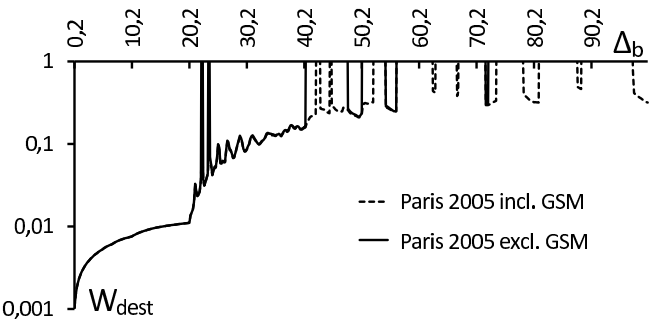

Figure 16: probability of destruction of an APC by a TCR as a function of the frequency shift Δ_b between consecutive quantum states in well (b), in Paris in 2005 including and excluding GSM.

Paris, in 2004 the Δ_b values corresponding to TCR-pMHC systems affected by the pro-autoimmune, anti-cancer effect of GSM are those for which there is an attenuation in the presence of GSM but not in the absence of GSM, on figure 15 . In Paris end 2005 these are heavily modified as shown on figure 16 . Many frequencies below 40 MHz were affected in 2004 are no more affected in 2005, and some of the frequencies above 40 MHz were un-affected in 2004 became affected in 2005. Some of the frequencies newly affected by GSM in 2005 in Paris were newly affected by permanent waves only in Nantes as shown of figure 8, including the 50.4 to 52.4 MHz frequency range. Any cancer recognized mostly by TCRs having a Δ_b amongst these frequencies newly affected by GSM in Paris and newly affected by permanent waves only in Nantes may have increased death rates in Nantes and decreased death rates in Paris upon start-up of DVB.

On figures 14, 15, 16 it was assumed that the frequency conditions 87 and 88 were respected by both the permanent waves (FM radio, TV) and the time-varying wave (GSM). Whenever this is not the case, the interaction of permanent waves and time-varying waves yields very different results. For example, if a T cell has a fundamental frequency F_{fund} of the (a) to (b) transition and a bandwidth of occupied states in well (a) Δ_{ath} which verify the frequency conditions 87 and 88 for GSM but not for FM radio and Television, then this T cell is affected by GSM in the same manner whether or not FM radio and TV signals are present, with an attenuation described by the "GSM

only" curve of figure 14.

9 Confirmation of the theory by death statistics

9.1 statistical methods

9.1.1 year to year variations of the number of deaths

The statistics in section 9.3 concern yearly numbers of deaths due to a specific cause in a specific age category. For estimating the significance of these figures the following procedure is followed:

- an estimate of the number of expected yearly deaths is computed based on the N previous years as

$$\lambda_N(y) = \frac{pop(y)}{N}\left(\frac{De(y-1)}{pop(y-1)} + \frac{De(y-2)}{pop(y-2)} \cdots + \frac{De(y-N)}{pop(y-N)}\right) \quad (103)$$

wherein $pop(y)$ is the population basis on which the number of deaths $De(y)$ is considered (for example, $pop(y)$ is the number of men in the 35-44 age range and $De(y)$ is the number of deaths by cancer in the same age range). When the population is unknown or not used, a constant value of $pop(y)$ is used in the equations.

- The probability of each integer number of deaths k occurring in the 35-44 age category is calculated by applying a Poisson law (which applies because each death is considered independent from the other and the population basis from which the number of deaths is extracted is large):

$$P_N(y,k) = e^{\lambda_N(y)}\frac{\lambda_N(y)^k}{k!} \quad (104)$$

- The probability of the number of deaths in the age class 35-44 being less than or equal to the number $De(y)$ of deaths actually observed is calculated as

$$P_{-,N}(y) = \sum_{k=0}^{De(y)} P_N(y,k) \quad (105)$$

- The probability of the number of deaths in the age class 35-54 being more than or equal to the number $De(y)$ of deaths actually observed is calculated as

$$P_{+,N}(y) = 1 - \sum_{k=0}^{De(y)-1} P_N(y,k). \quad (106)$$

- $P_{+,N}(y)$ and $P_{-,N}(y)$ sometimes depend strongly on N. To avoid considering a result as significant where it is significant only for a specific value of N, the maximum value over $N = 1$ to 6 of the above probabilities are calculated:

$$P_-(y) = \max_{N=1\cdots6} P_{-,N}(y) \quad (107)$$

$$P_+(y) = \max_{N=1\cdots6} P_{+,N}(y) \quad (108)$$

- A decrease of the number of deaths is considered significant when $P_-(y) < 0.05$. An increase of the number of deaths is considered significant when $P_+(y) < 0.05$.

9.1.2 reported deaths in a specific age category

In section 9.2 the exact number of deaths in each age category is unavailable. What is available is a number of reported deaths in each age category, with unknown variable reporting rate. In this section the significance of the results is estimated as follows:

- For each considered one-year period an estimate λ of the probability of a reported death being in the 35-54 age category is calculated for the group of cities which did not receive an emitter (Chateaubriant, Cholet, Ancenis, Challans, La Flche) by dividing the total number of reported deaths in the age category 35-54 in all cities, by the total number of reported deaths in the same cities.

- The probability of each integer number of deaths k occurring in each city in the 35-54 age category is calculated by applying a Bionomial law

$$P_{bin}(k) = C_n^k \lambda^k (1-\lambda)^{(n-k)} \quad (109)$$

with n the total number of reported deaths. The Binomial distribution applies because the deaths in the 35-54 age category are assumed to occur in a random manner amongst the total number of reported deaths.

- The probability of the number of deaths in the age class 35-54 being less than or equal to the number De of deaths actually observed is calculated as

$$P_-(De) = \sum_{k=0}^{De} P_{bin}(k) \quad (110)$$

.

- The probability of the number of deaths in the age class 35-54 being more than or equal to the number De of deaths actually observed is calculated as

$$P_+(De) = 1 - \sum_{k=0}^{De-1} P_{bin}(k) \quad (111)$$

- These calculations are carried out for each one-year period starting at day -135 to +720 by steps of 45 days.

- The minimum values of P_+ and P_- over all one-year periods is computed (Table 3).

9.2 death synchronization by DVB startup

I used death notices published in local newspapers [1] to conduct surveys of deaths as correlated to the installations of DVB emitters in various cities. About a half of the deaths of most surveyed cities are reported in these documents, in a manner essentially independent from the exact cause of death. For each surveyed city, I computed at 45 days intervals the yearly number of deaths in the 35 to 54 years old age class, divided by the total number of deaths reported. This method partially avoids bias due to changing seasons and varying rates of reporting. The death notices were available from 06/2009 onward.

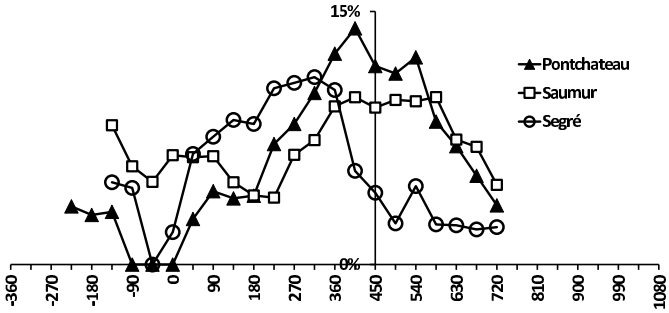

Figure 17: ratios of yearly mortality in the 35-54 years age range over total yearly mortality, as a function of time (in days), for places having received DVB emitters authorized by the ANFR (Agence Nationale des Fréquences) on 5th February 2010 and having discontinued analog TV emission on 18th may 2010 in the region "Pays de Loire", with a starting date on 5th February 2010.

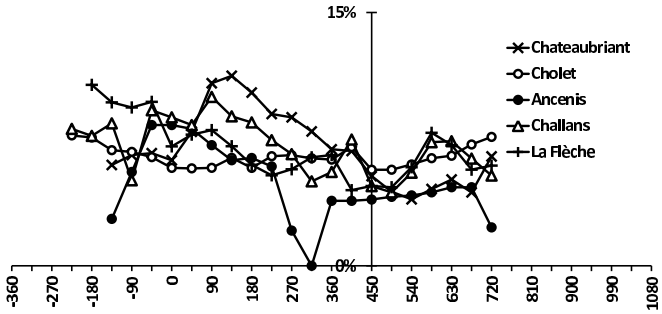

Figure 18: ratios of yearly mortality in the 35-54 years age range over total yearly mortality, as a function of time (in days), for places not having DVB emitters in the region "Pays de Loire", with a starting date (day 0) corresponding to the full year starting on 5th February 2010. Only La Fleche had analog emitters, which were shut down on may 18th 2010.

In the region of Pays de la Loire 3 sets of DVB emitters were authorized on 05 february 2010 [10] and installed shortly thereafter in cities which previously did not have any DVB emitter. Then on may 18th 2010 the analog emitters were shut down. The corresponding curves are shown on figure 17. The horizontal scale is in number of days from the emitter installation to the beginning of the one-year period on which deaths are summed up. Each curve shows a maximum which is reasonably coincident,the differences possibly reflecting the differences in medical practice between different hospitals. For comparison, figure 18 shows the same curves for comparable cities in the same area which did not receive an emitter. None of these cities shows a maximum in the referenced period. So there is clearly a correlation between the installation of a DVB emitter and an increased death rate in the 35-54 age class in a period of one year starting between days 270 and 450 after installation of the DVB emitter. Figure 19 shows the averaged curves of the group of cities which received an emitter (Pontchateau, Saumur, segré) and the averaged curve of the group of cities which did not receive an emitter (Chateaubriant, Cholet, Ancenis, Challans, La Fleche). The group of cities which received an emitter shows a mortality peak as compared to the group of cities which did not receive an emitter. This group of cities also show a mortality minimum prior to the peak.

The significance of these results was evaluated as discussed in section 9.1.2 (Table 3).

The probability P_+ corresponding to the maximum mortality in age category 35-54 passed the significance threshold of 0.05 in Pontchateau and Saumur and was fairly near threshold (0.07) in Segré, but did not pass the threshold in any other city (minimum 0.13 in Chateaubriant). For the group of cities Pontchateau, Saumur, Segré the probability passed the significance threshold of 0.01 . These results show that the mortality maximum in the group of cities having received a DVB emitter is significant as compared to the group of cities that did not receive a DVB emitter. They also show that this mortality maximum is individually significant in each city having received an emitter except possibly the case of Segré which is open

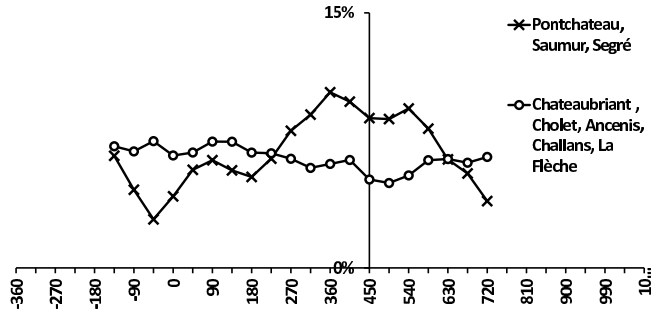

Figure 19: averaged ratios of yearly mortality in the 35-54 years age range over total yearly mortality, as a function of time (in days), for places having received a DVB emitter or not having received a DVB emitter in the region "Pays de Loire", with a starting date on 5th February 2010.

	min P+	*min P+ starting day*	min P-	*min P- starting day*
Chateaubriant	0,138	*135*	0,244	*675*
Cholet	0,218	*720*	0,138	*90*
Challans	0,194	*90*	0,363	*-90*
La Flèche	0,211	*-90*	0,247	*405*
Ancenis	0,429	*0*	**0,048**	*315*
Pontchateau	**0,034**	*540*	0,123	*-45*
Saumur	**0,020**	*495*	0,141	*225*
Segré	0,076	*315*	**0,028**	*-45*
Pontchateau, Saumur, Segré	**0,008**	*360*	**0,008**	*-45*

Table 3: Minimum values of P_+ and P_- for various cities and for a group of cities, and starting day of the corresponding one-year period

to discussion. This implies that the cause for the increase is a common cause to Pontchateau, Saumur, Segré. Since the installation of a DVB emitter is the only identified difference between on the one hand Pontchateau, Saumur, Segré and on the other hand Chateaubriant, Cholet, Ancenis, Challans, La Fleche , it is most likely the cause of the mortality maximum.

The probability P_{-} corresponding to the minimum mortality passed the significance threshold of 0.05 in Ancenis, for a non-identified reason. It also passed the significance threshold of 0.05 in Segre, but not in Pontchateau or Saumur. However for the group of cities Pontchateau, Saumur, Segre the significance threshold of 0.01 was passed. These figures show that the mortality minimum in the group of cities of Pontchateau, Saumur, Segre is significant as compared to the other group of cities, but do not give a clear response to the question of whether this minimum was due to a common cause in Pontchateau, Saumur, Segre.

This synchronism is believed to be due to the perturbation of the immune system due to the transitions between different exposures.

The mortality peak is likely to be mostly by cancer (this will be justified further in section 9.3), the delay from emitter authorization to death being due to the time for cancer development as lengthened by medical efforts. This is in full agreement with the theory summarized inter alia in Table 2. DVB is essentially a gaussian signal with constant average amplitude so that the conclusions of part 6 apply very directly here. The surveyed cities are small so there is no significant amplitude variation due to weather changes. In each location all DVB emitters were installed simultaneously. So the period immediately after installation is pro-cancer according to Table 2 column C. In all cases, at least 4 emitters (resulting in 4 multiplexes of 8 MHz bandwidth each being broadcast) were installed. I measured the DVB power in Pontchateau to be below 10^{-6} W/m2 (per 8 MHz - wide DVB multiplex) everywhere, taking into account a margin of error. Taking into account the presence of 5 multiplexes, the power threshold is somewhere below $5 \cdot 10^{-6}$ W/m2 for T cells recognizing cancerous cells, for a significant part of cancers and of the population.

Nantes is the capital city of the "Pays de la Loire" region, with more than 200.000 inhabitants. The curves based on the 35-54 age range are dominated by the 45-54 age class and do not show a significant change in mortality in Nantes. Figure 20 shows the synchronized curves calculated for the 35-44 age range for Nantes, for the group of (Pontchateau, Saumur, Segré) which received an emitter, and for the group of (Chateaubriant, Cholet, Ancenis, Challans, La Fleche) which did not receive an emitter. As compared to figure 19, the ratio between the curves of (Pontchateau, Saumur, Segré) and (Chateaubriant, Cholet, Ancenis, Challans, La Fleche) is increased, showing a preferential effect on this age group. This preferential effect could be due to a delay between full thymus involution and start-up of other means for generating mature naive T-cells (extra-thymic T cell generation is known to exist exists). The curve for Nantes for the 35-44 years age group shows an increase of mortality which is substantially

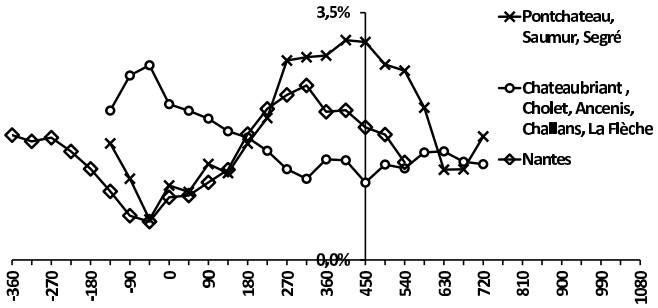

Figure 20: ratios of yearly mortality in the 35-44 years age range over total yearly mortality, as a function of time (in days). The curve of Nantes has a starting date on 4th june 2010 approximately corresponding to the increase in authorized power in the corresponding emitter of Haute-Goulaine. The other places have a starting date on 5th February 2010 corresponding to authorization of the emitters of Pontchateau, Saumur, segré.

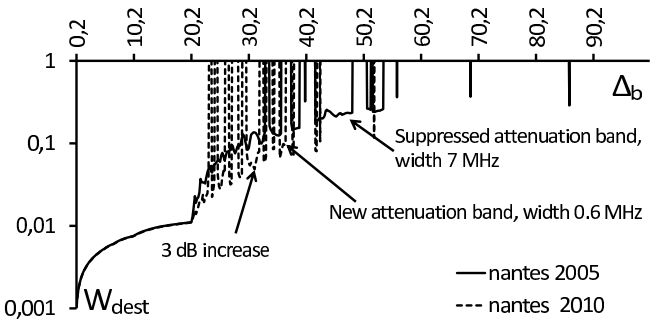

Figure 21: probability of destruction of an APC by a TCR as a function of the frequency shift Δ_b between consecutive quantum states in well (b), in Nantes prior to and after extinction of analog TV emitters and power increase of DVB multiplexes.

coincident with the increase of mortality in (Pontchateau, Saumur, segré) but which stops earlier and yields to a substantially lower peak.

The curve of Nantes on figure 20 is synchronized with respect to the date of an authorization for increase of emission power which substantially coincided with the abandonment of analog emissions. Emission power was about doubled at that date. The authorized power for each multiplex R1, R2, R3, R4, R6 was 34 kW, and was increased to respectively 98, 43,65,83,65 kW. The center frequencies of the multiplexes were rearranged. Analog emissions were abandoned. Some emitters were however changed about 6 months earlier so in practice it is unclear whether some of the power increase happened earlier - which would shift the Nantes curve 180 days to the right -. Figure 21 shows the destruction probability W_{dest} of the TCR-pMHC systems in Nantes as a function of their Δ_b before and after the change calculated as in section 6.18. For some Δ_b values the W_{dest} was decreased yielding to a pro-cancer transient situation, for others it was increased yielding to an anti-cancer, pro-autoimmune situation. The anti-cancer effects may affect different T cells than the pro cancer effects as they correspond to different values of Δ_b.

All single-city curves including the curve of Nantes show

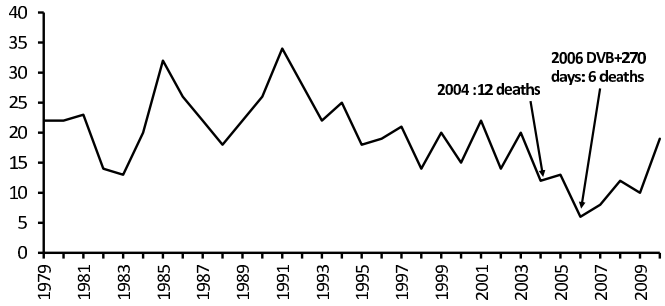

Figure 22: yearly number of deaths in the 35-44 years age range for men only in Paris corresponding to neoplasms of the lung, trachea and bronchial tubes

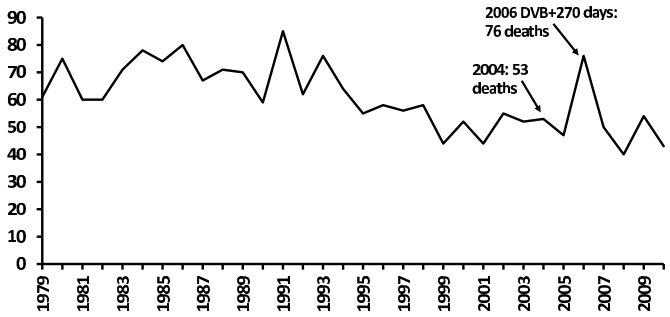

Figure 23: yearly number of deaths in the 35-44 years age range for men only in Paris corresponding to neoplasms excluding neoplasms of the lung, trachea and bronchial tubes

that the peak mortality period is preceded by a period of unusually low mortality. Due to the preceding period of unusually low mortality, it is unclear whether the curves of Pontchteau, Saumur, segré for the 35-54 years age range yield to a net increase of the number of deaths when integrated over time. The curves for the 35-44 years age range are much more likely to yield to a net increase in the total number of deaths. These curves are dominated by the men's death rate which is much higher than women's death rate in these age classes. Therefore the chances to find a net increase in official statistics are maximized by examining the statistics for men in the 35-44 age range.

The reduction of exposure (and possibly associated reduction in cancer mortality) due to the extinction of the analog emitters may have played a role in the preceding period of low mortality not only in Nantes but also in Pontchateau, Saumur, Segré since the analog emitters were shut off simultaneously in all theses cities.

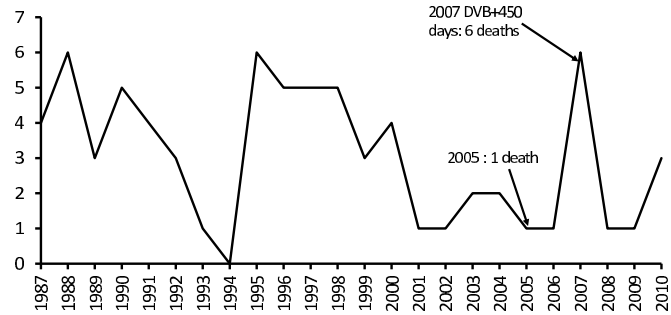

Figure 24: yearly number of deaths in the 35-44 years age range for men only in Nantes corresponding to neoplasms of the lung, trachea and bronchial tubes

9.3 causes of death upon DVB startup

The curves in section 9.2 do not give any direct insight into the causes of the deaths. These causes can be better understood by using the yearly statistics on causes of death [15] for the years prior to and after the first installation of the DVB emitters, in march 2005 in Paris and september 2005 in Nantes.

It has been found that the group of neoplasms comprising neoplasms of the larynx, trachea, bronchial tubes and lung (group A) behaves differently than other neoplasms (group B). Group A reacted negatively to the onset of DVB in Paris (figure 22): the number of group A cases was about divided by 2 in 2006. Group B reacted positively (figure 23): the number of group B cases increased by 60 % in 2006 as compared to the previous year. Both the decrease of group A and the increase of group B were statistically significant (values of P_+ and P_- are in Table 5). The resulting increase of the "all cancers" cases was also significant.

In Nantes, both groups reacted positively (figures 24 and 25). The increase of group A neoplasms was statistically significant ($P_+ = 0.005$), the increase of group B neoplasms was not.

The abnormal behaviour of group A neoplasms in Paris in the age class 35-44 may for example be due to:

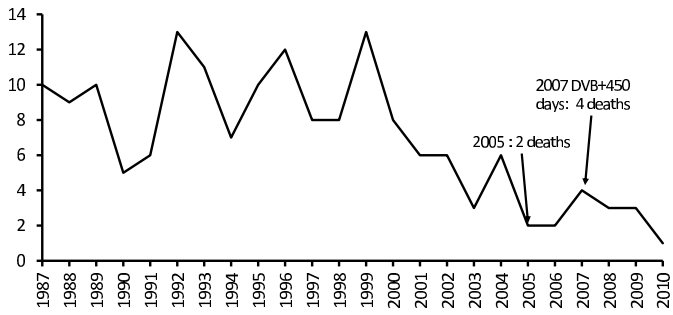

Figure 25: yearly number of deaths in the 35-44 years age range for men only in Nantes corresponding to neoplasms excluding neoplasms of the lung, trachea and bronchial tubes

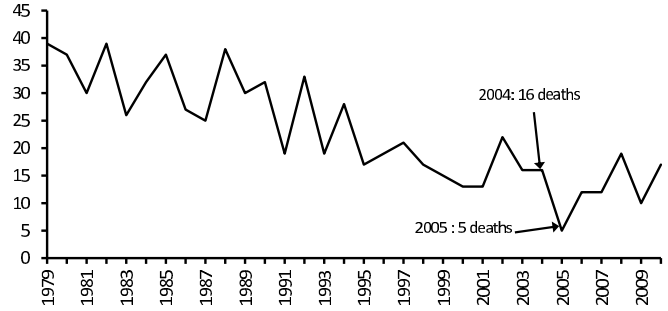

Figure 26: yearly number of deaths in the 35-44 years age range for men only in Paris by heart disease

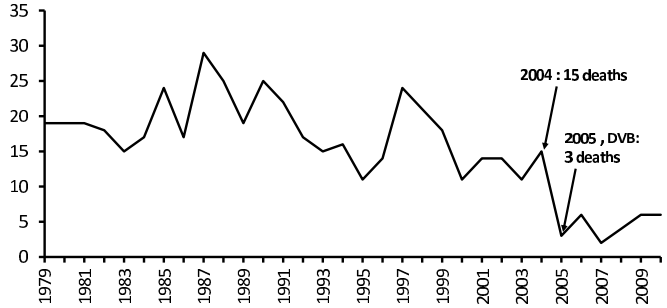

Figure 27: yearly number of deaths in the 35-44 years age range for men only in Paris by chronic disease of the liver

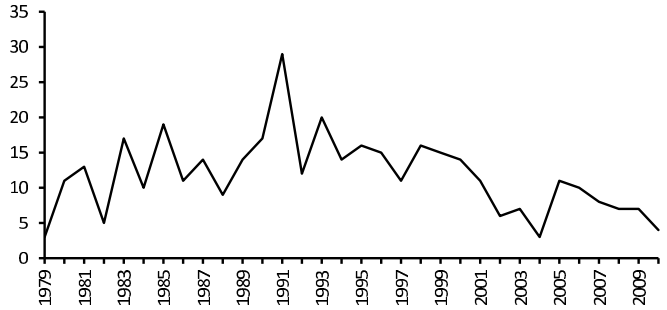

Figure 28: yearly number of deaths in the 35-44 years age range for men only in Paris by infectious diseases excluding AIDS

- a different interplay of effector T cells and regulator T cells due to a different exposure history, or

- to inhibitory receptors of the T cells implied in the control of group A neoplasms being affected by the changes in Paris but not in Nantes: if inhibitory receptors are affected in a manner similar to TCR-pMHCs and become unable to bind their target, an anti-cancer effect may appear.

- to these neoplasms being mostly controlled by TCRs having a Δ_b amongst the frequencies newly affected by GSM or other time-varying waves in Paris in 2005 but not in Nantes, as described in section 8.

- to an associated inflammatory reaction being simultaneous with the cancer and the direct final cause of death. The transition being anti-inflammatory can also result in a decreased number of deaths in this case. There may be a specific pollutant in Paris causing an inflammatory response which is less present in Nantes.

Concerning women it was found that the most sensitive age group was 55-64. The number of group A neoplasms in this age group for women increased by 22 % in 2006 with respect to the previous year. The increased level (which was also the highest since 1979) was maintained until 2009, perhaps revealing a slower generation of new T cells due to age. Group B did not react at all in this case.

Cancer is not the only cause of death which was affected by the start-up of DVB broadcasting. Figures 26 and 27 show statistically significant decreases in the numbers of deaths for heart diseases and chronic diseases of the liver (P_- is in Table 5). Detailed examination of the data reveals a temporary decrease (only in 2005) of deaths by acute myocardial infarction, and a longer term decrease of cardiomyopathy and alcoholic liver disease.

Autoimmune or inflammatory effects may play a role in these diseases, which would explain the decrease on the basis of Table 2 columns B or C.

Data for women aged 55-64 also show a decrease of heart diseases and liver diseases but in this case the effect is transient, including on liver diseases.

The yearly deaths by infectious diseases also increased in 2005 (figure 28) in good agreement with Table 2 columns B and C. After the initial increase, the number of deaths decreased only progressively each year, in agreement with Table 2 column B which predicts a long term increase. The statistical significance of this increase is uneasy to assess because infectious diseases are not expected to follow a Poisson's law: deaths tend to occur by clusters due to the infectious nature of the disease, rather than independently from each other as requested for the application of Poisson's law.

Table 4 summarizes all of the above statistically significant variations of death causes in Paris in 2005-2006 for men aged 35-44 years. Death by infectious diseases was incorporated in this table both because it was expected and because it is an unusual increase.

Table 4 confirms that the above-mentioned variations of death causes resulted in a decrease of mortality in 2005 and an increase of mortality in 2006 so that the exceptional variations alone do yield to a synchronization effect as observed and discussed in section 9.2. The variation of all known causes of death excluding AIDS was -10 % between 2004 and 2005 and +10% between 2004 and 2006. 80 % of these variations is accounted for by the exceptional variations of Table 4 and a further 20 % of the increase represents the contribution of other known causes. Whilst one or the other statistically significant changes may be due to something else than the start-up of DVB broadcasting, it is most unlikely that the whole picture, including the statistically significant variations concerning half of the deaths in Paris in 2004-2006 and the death synchronization effects observed in Nantes and elsewhere in 2009-2011 are due to chance. These variations are thus due to perturbation of the immune system due to changes in TV broadcasting, confirming the theories described herein.

Table 4 also explains the shape of the curves of section 9.2. The initial decrease of the death rate followed by an increase in the year starting on day 450 after emitter installation corresponds roughly to the decrease of known

	ICD-10 classes	Number of deaths 2004, not affected by exceptional variations	Number of deaths 2004, affected by exceptional variations	exceptional variation 2004 to 2005	exceptional variation 2004 to 2006	exceptional percentage variation 2004 to 2005	exceptional percentage variation 2004 to 2006
Neoplasms	C00-D48						
of which: neoplasms of the larynx, trachea, bronchial tubes and lung	C32-C34		12		-6		-50%
of which: other neoplasms			53		23		43%
heart disease	I20-I25; I30-I33; I39-I52		16	-11		-69%	
chronic illness of the liver	K70; K73-K74		15	-12	-9	-80%	-60%
infectious diseases	A00-B99						
of which: AIDS	B20-B24	37					
of which: non-AIDS			3	8	7	267%	233%
accidents	V01-Y89 excl. X60-X84	18					
mental problems	F00-F99; X60-X84	17					
disease of the nervous system	G00-H95 exc. G03	5					
other known causes		19					
TOTAL		96	99				
exceptional decrease				-23	-15		
exceptional increase				8	30		
net exceptional variation				-15	15		

Table 4: known death causes in Paris following the onset of DVB for men aged 35-44 years

causes of death in Paris in 2005 and their increase in Paris in 2006. The 2006 peak in Paris was largely due to cancer, confirming that the peaks in Pontchateau, Saumur, Segré were most likely dominated by cancer.

The significance of these results was verified as discussed in section 9.1.1 (Table 5)) except for deaths by infectious diseases because deaths by infectious diseases are not expected to follow a Poisson's law: deaths tend to occur by clusters due to the infectious nature of the disease, rather than independently from each other as requested for the application of Poisson's law.

The values for 2005-2006 confirm that the decreases of heart diseases and liver diseases in 2005 are statistically significant, and that the increase of death by neoplasm, the increase of death by neoplasm excluding larynx, trachea, bronchial tubes and lung (group B neoplasms), and the decrease of death by neoplasm of the larynx, trachea, bronchial tubes and lung (group A neoplasms) in 2006 are in each case significant.

This table also makes possible a retrospective analysis of other years. In 1995 there was the only significant year-to-year decrease of death due to neoplasms in the entire period 1980 to 2010. This follows the major development of GSM in France in 1994 with the number of GSM users being multiplied by 7 in a single year and becoming higher than the number of users of analog radio-telephony. In 1991 there was a significant increase of deaths due to neoplasms and a significant decrease of heart diseases. The cause for the 1991 change is not identified. During the 14 years immediately preceding 2006 there was no statistically significant increase of death by all neoplasms.

9.4 decrease of cancer mortality by GSM and other time-varying electromagnetic waves

Theory predicts that time-varying signals like GSM may have an anti-cancer effect (Table 2, column E). Figure 29 shows variations of the age-specific death rates attributed to all neoplasms in France for men. The 35-44 years age category, which was already identified as the most sensitive category in relation to the onset of DVB, had a strongly diminishing cancer death rate during from 1998 onwards corresponding to a period in which time-varying communication networks including GSM-900, GSM-1800, UMTS, Wifi were strongly developed. "time-varying" means here that these networks result in that a majority of the population is subject to exposure variations due for example to:

(a) day/night load variations of GSM or UMTS base stations.

(b) spending time in the vicinity of emitters and other time away from emitters: in-house movements relative to the position of a wifi emitter, working day / night movement between different cellular phone base stations exposures.

(c) temporary exposure to GSM or DECT pulses or to UMTS when making a call or when being near someone who is calling.

Younger age categories were not clearly affected as they were already on a regular decrease since the 1960s. Older

	neoplasm excl. Larynx, trachea, bronchial tubes and lung			neoplasm of the larynx, trachea, bronchial tubes and lung			all neoplasms			heart disease			chronic disease of the liver		
	number	P- (decrease)	P+ (increase)	*number*	P- (decrease)	P+ (increase)	*number*	P- (decrease)	P+ (increase)	*number*	P- (decrease)	P+ (increase)	*number*	P- (decrease)	P+ (increase)
1979	*61*			*22*			*83*			*39*			*19*		
1980	*75*	0,965	0,045	*22*	0,556	0,528	*97*	0,941	0,072	*37*	0,415	0,647	*19*	0,561	0,531
1981	*60*	0,182	0,967	*23*	0,637	0,444	*83*	0,250	0,932	*30*	0,141	0,920	*19*	0,561	0,531
1982	*60*	0,534	0,835	*14*	0,041	0,983	*74*	0,176	0,962	*39*	0,954	0,290	*18*	0,469	0,622
1983	*71*	0,928	0,244	*13*	0,464	0,965	*84*	0,887	0,543	*26*	0,082	0,989	*15*	0,287	0,837
1984	*78*	0,965	0,218	*20*	0,975	0,421	*98*	0,983	0,081	*32*	0,896	0,670	*17*	0,749	0,625
1985	*74*	0,813	0,690	*32*	1,000	**0,008**	*106*	0,989	0,222	*37*	0,938	0,315	*24*	0,978	0,094
1986	*80*	0,922	0,338	*26*	0,930	0,877	*106*	0,965	0,513	*27*	0,234	0,963	*17*	0,423	0,944
1987	*67*	0,367	0,938	*22*	0,640	0,923	*89*	0,410	0,958	*25*	0,398	0,917	*29*	0,997	**0,044**
1988	*71*	0,714	0,683	*18*	0,289	0,969	*89*	0,528	0,883	*38*	0,994	0,123	*25*	0,888	0,796
1989	*70*	0,579	0,695	*22*	0,855	0,721	*92*	0,650	0,728	*30*	0,548	0,920	*19*	0,371	0,956
1990	*59*	0,117	0,962	*26*	0,922	0,368	*85*	0,323	0,894	*32*	0,685	0,657	*25*	0,927	0,473
1991	*85*	0,999	**0,047**	*34*	0,994	0,075	*119*	1,000	**0,008**	*19*	**0,019**	0,997	*22*	0,556	0,753
1992	*62*	0,174	0,996	*28*	0,800	0,869	*90*	0,334	0,998	*33*	0,999	0,299	*17*	0,169	0,944
1993	*76*	0,964	0,401	*22*	0,318	0,962	*98*	0,816	0,751	*19*	0,097	0,997	*15*	0,371	0,967
1994	*64*	0,299	0,927	*25*	0,777	0,740	*89*	0,326	0,917	*28*	0,980	0,562	*16*	0,664	0,868
1995	*55*	0,143	0,982	*18*	0,150	0,975	*73*	**0,047**	0,997	*17*	0,104	0,990	*11*	0,154	0,982
1996	*58*	0,688	0,909	*19*	0,651	0,923	*77*	0,706	0,966	*19*	0,736	0,897	*14*	0,854	0,840
1997	*56*	0,509	0,917	*21*	0,764	0,778	*77*	0,620	0,939	*21*	0,799	0,704	*24*	0,999	**0,033**
1998	*58*	0,638	0,704	*14*	0,133	0,974	*72*	0,364	0,916	*17*	0,378	0,913	*21*	0,911	0,757
1999	*44*	**0,048**	0,991	*20*	0,952	0,515	*64*	0,189	0,977	*15*	0,371	0,910	*18*	0,670	0,856
2000	*52*	0,898	0,714	*15*	0,371	0,895	*67*	0,675	0,846	*13*	0,363	0,951	*11*	0,073	0,994
2001	*44*	0,313	0,924	*22*	0,967	0,190	*66*	0,557	0,764	*13*	0,573	0,865	*14*	0,854	0,881
2002	*55*	0,954	0,357	*14*	0,225	0,972	*69*	0,688	0,587	*22*	0,992	0,104	*14*	0,725	0,836
2003	*52*	0,710	0,675	*20*	0,952	0,349	*72*	0,772	0,382	*16*	0,591	0,923	*11*	0,353	0,951
2004	*53*	0,725	0,545	*12*	0,135	0,979	*65*	0,407	0,811	*16*	0,586	0,785	*15*	0,907	0,517
2005	*47*	0,370	0,825	*13*	0,682	0,873	*60*	0,293	0,867	*5*	**0,002**	1,000	*3*	**0,001**	1,000
2006	*76*	1,000	**0,001**	*6*	**0,035**	0,999	*82*	0,997	**0,036**	*12*	0,998	0,798	*6*	0,966	0,971
2007	*50*	0,300	0,999	*8*	0,847	0,976	*58*	0,101	0,998	*12*	0,909	0,756	*2*	0,174	1,000
2008	*40*	0,086	0,999	*12*	0,973	0,557	*52*	0,238	0,989	*19*	0,998	0,108	*4*	0,947	0,970
2009	*54*	0,986	0,589	*10*	0,745	0,758	*64*	0,955	0,558	*10*	0,347	0,991	*6*	0,966	0,678
2010	*43*	0,311	0,958	*19*	0,999	**0,018**	*62*	0,727	0,615	*17*	0,986	0,289	*6*	0,889	0,554

Table 5: Number of deaths for men in the 35-44 age category in Paris and values of P_+ and P_- by year and cause of death. Significant values below 0.05 and years of interest are underlined.

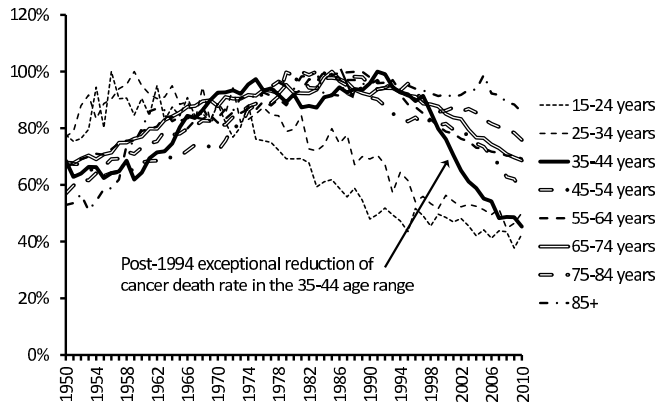

Figure 29: normalized age-specific death rates due to neoplasms for men in France by age category

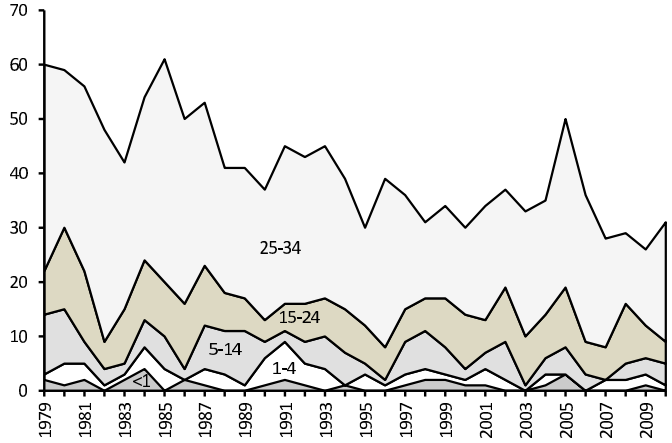

Figure 30: number of deaths due to neoplasms in Paris for men in younger age groups

age categories were affected in a more moderate manner.

This exceptional decrease in cancer death rate in the 35-44 age category for men confirms that time-varying artificial electromagnetic waves have a permanent anti-cancer effect in accordance with Table 2 column E. It took some time for the drop of cancer death rate to become significant nationwide after the onset of GSM, but in Paris, where the concentration of GSM users is higher, the drop was significant on a year-to-year basis in 1995 (table 5) corresponding to the major development of GSM-900 in 1994, so that it can reasonably be concluded that GSM-900 triggered the initial drop.

9.5 age patterns of cancer in men

The pro-cancer effect illustrated by figure 23 and the anti-cancer effect illustrated by figure 29 have a marked dependency on age.

The transition from low to high exposure (Table 2 column C) results in existing T cells becoming momentarily unable to control the cancer. In younger subjects before thymus involution, this results in favouring neoplasms which grow sufficiently fast to pass a size threshold before the end of the transition period, from which the immune system can no more control them even after activation of efficient new T cell lines. As subjects get nearer to the age of thymus involution, the transition period becomes longer and more slowly developing neoplasms are favoured. This hypothesis is supported by Figure 30 which shows that in the younger than 34 age categories the number of deaths by cancer increased in 2005, unlike the number of cancer deaths in the 35-44 age category which increased only in 2006.

Older age categories responded less to the increase in time-variable waves as shown on figure 29. However this lower response is not absolutely general. Whilst in Nantes (or in Paris in 2005) the exceptional variation of the death rate affects exclusively the 35-44 age range, in small cities like Pontchateau, Saumur, Segré it also affects the 45-54 age range (figure 31). The reason for this different behaviour is somewhat unclear, but a result is that the percentage increase in the number of deaths in the peak year was a lot higher in these small cities than in larger cities.

This difference between small and large cities may be linked to the general fact that the impact on cancer deaths of a change in the electromagnetic environment depends on the pre-existing electromagnetic environment. In Paris and Nantes in 2005 the pre-existing environment was particularly crowded, in particular the FM band was almost fully occupied and there was an analog TV emission in the VHF band ("Canal +"). These emissions may be of importance both because of their high bandwidth and because of their also high Rabi integration bandwidth (see table 1 for FM), which results in an extension of their effects to neighbouring frequencies. The FM band was generally much less crowded in small cities and in Pontchateau and Segre there was no analog TV emitter in the VHF band. The addition of the same digital channels had a stronger impact when applied on a less crowded pre-existing electromagnetic environment because the relative change was stronger. Comparison of figure 10 with figure 9 shows that in Thorens-Glires, a small city with no local FM emitter, the low frequency Δ_b range from 0 to 20 MHz was strongly affected by the onset of DVB, whilst it was almost un-affected in Nantes and Paris. This contrast between small and large cities is further increased if we take into account the extended Rabi frequencies of strong FM emitters. As the impact of the change is generally stronger, the older age categories are also more likely to be affected.

In the case of time-varying exposure (Table 2 column E and figure 29) the impact of exposure on death rate is maximum in the 35-44 age class and diminishes in older age classes. The lower impact in older age classes is most likely due to the reduction of thymus output: the likelihood of selecting a T cell under time-varying exposure which is efficient against a line of cancerous cells is proportional to thymus output.

10 Confirmation of the theory with experimental therapeutical results

A device described in [4] [11] was used successfully to cure cancer in the 1930s [41] [33]. This device essentially emits

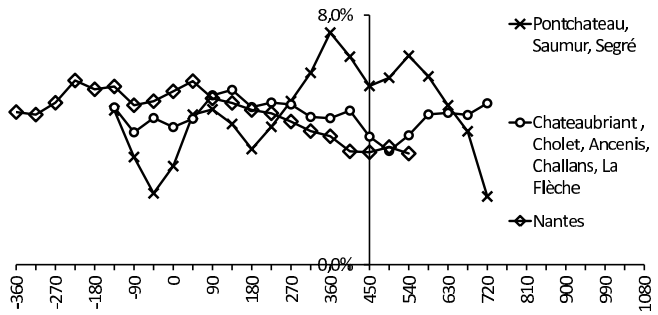

Figure 31: ratios of yearly mortality in the 45-54 years age range over total yearly mortality, as a function of time (in days). The curve of Nantes has a starting date on 4th june 2010 approximately corresponding to the increase in authorized power in the corresponding emitter of Haute-Goulaine. The other places have a starting date on 5th February 2010 corresponding to authorization of the emitters of Pontchateau, Saumur, segré.

a broadband signal. The patients were typically exposed 15 minutes, the exposure being repeated a few times at intervals of a few days, thus creating a few high exposure periods during which the patient's thymus produced abnormally aggressive cells. The T cells that passed negative selection steps in the thymus during the high exposure period with peptides abnormally displayed by neoplasm cells (or similar to such abnormally displayed peptides) were abnormally aggressive against the neoplasm after leaving thymus and could thus control the neoplasm, resulting in a mechanism which is essentially as described in Table 2 column E. There was no appropriate theoretical framework to explain these results at the time, however the facts were recorded and are a strong experimental confirmation of the present theory.

11 Consistency of the theory with some decreased cancer rates of cellular phone users

In the United states before 1998 the cell phone market was dominated by AMPS, which is an analog cell phone, D-AMPS, which is pulsed with a pulse length of 6 miliseconds, and CDMA, which is digital but not pulsed. Use of cell phones was found to diminish the incidence of brain cancer in two studies conducted in the US between 1994 and 1998 [29] [38]. This result is in full agreement with Table 2 column E. The increased exposure power during call-time caused the thymus to produce abnormally aggressive T-cells which had an anti-cancer effect when the phone user was un-exposed, resulting in diminished incidence of brain cancer in mobile phone users.

The GSM standard uses 124 frequency sub-carriers and each sub-carrier uses TDMA. Each individual communication uses pulses lasting 0.57 milliseconds at a repetition rate of 4.62 milliseconds on a sub-carrier having a 200 kHz bandwidth. For the present theory to apply directly to the signal emitted by a single mobile phone, τ_{rec} and τ_{bind} (as defined in section 6) must ideally be smaller than the pulse duration of 0.57 ms, so that the GSM signal can at least cancel an entire positive selection step in the thymus. This figures is below the evaluation of τ_{rec} in [40] which is 2.5 to 62.5 milliseconds. Therefore it is uncertain whether exposure to the signal of a single GSM mobile phone can result in cancelling any negative selection step and thus reducing incidence or cancer death rate.

However the "Interphone" international study in which GSM was the dominant standard to which subjects were exposed [23] confirmed that "moderate" GSM phone users also had a diminished brain cancer incidence as compared to non regular users. Therefore it is expected that τ_{bind} and probably τ_{rec} is less than 0.57 ms for at least some (possibly most) of the TCRs which are able to recognize cancerous cells.

[23] suggests that the strongest decrease could be for users having a cumulative call time below 5 hours during the 1 to 4 years before reference date because these users have an Odds Ratio of 0.68 with 95% confidence interval of 0.5-0.93 which is both significant and lower than most figures concerning more intense use. This is further confirmed by the fact that in a North European sub-study of Interphone the odds ratio of glioma in relation to ever use of a mobile phone was 0.63 (never users being the reference group) whilst it was only 0.78 for regular use (never users and non regular users being the reference group) [32]. It is further confirmed by a lower (though not significant) incidence of brain cancer for low latencies in [42] [30]. This may be due to two factors:

(a) a relatively minimal exposure time may be sufficient to maximize the anti-cancer effect by generating any aggressive T cells which can reasonably be generated by exposure, after which further exposure does not improve the situation. This explains why more frequent exposures do not further decrease the incidence of brain cancer.

(b) the anti-cancer effect may be stronger when exposure is infrequent because otherwise regulatory mechanisms may appear, including more numerous regulatory T cells, so as to eliminate uselessly aggressive T cells. Such mechanisms are likely to diminish the anti-cancer effect "normal" users as compared to "very moderate" or very recent users.

The fact that "very moderate" or very recent users may have an abnormally diminished probability of being diagnosed with brain cancer makes overall results of such studies extremely sensitive to the choice of the reference group. The inclusion in the reference group of users having up to 39 hours cumulative call time is probably the underlying cause of the finding of a generally increased incidence of brain cancer in mobile phone users in [27].

The generally diminished incidence of brain cancer in mobile phone users is further confirmed in [42] where it is found that it was found that a cohort comprising both NMT and GSM users had an significantly reduced brain cancer risk after 10 years latency as compared to the general population. The reason why there was not a comparable reduction of brain cancer for shorter latencies in this study is probably because the reference group was the general population rather than non-users, and the general population was widely equipped with GSM at the end of the follow-up period.

12 Consistency of the theory with observations near cell phone base stations

Exposure to a GSM base station differs very notably from exposure to an individual GSM phone. Residents living near a GSM base station are exposed full-time rather than part-time. In the hypothetical case of a permanently overloaded GSM base stations permanently using all available frequency sub-carriers and all available time slots, the signal transmitted by such base station is quite similar to a gaussian signal having a constant envelope and therefore when this hypothetical overloaded base station is turned on for the first time, residents living nearby are submitted to a pro-cancer effect due to the low to high transition as per Table 2 column C.

In practical cases the load of a base station is variable. However near to the base station the signal power is ordinarily far superior to 10^{-4} W/m2 and, based on Table 1, the Rabi integration bandwidth is expected to be higher than the GSM bandwidth. Therefore all individual Rabi frequencies corresponding to individual sub-carriers merge and formula 95 applies with Δ_{art} being replaced at any time by $\Delta_{gsm} = N_{gsm} \cdot \delta_{gsm}$ expressed in Hz wherein N_{gsm} is the number of sub-carriers simultaneously in use (i.e. on which there is an ongoing pulse) and with P_{art} being the total emitted power, summed up on all 124 sub-carriers. The number of sub-carriers simultaneously in use varies, inter alia with load, but rarely goes to zero, and therefore the attenuation of W_{dest} due to the base station signal varies with load but is rarely canceled. Even at zero load there is still a signalling channel active. Since the signal is only rarely canceled, it can be viewed as a mix of a constant background, yielding a transient pro-cancer effect as per Table 2 column C, and of a variable signal, yielding a permanent anti-cancer effect as per Table 2 column E. At start-up of the base station some T cell lines which previously controlled cancer suddenly become unable to bind their corresponding pMHC, so that the transient pro-cancer effect dominates.

In [47] the incidence of cancer cases near a cell phone base station was studied from 1 year after the onset of the cell phone base station to 2 years after the onset. The cell phone base station came into service in 7/96 and was GSM or GSM-like. Cancer incidence was abnormally high as compared to both a nearby area and the general population. 7 out of 8 cancer victims near the cell phone base station were women. It is not specified whether victims recovered or died. The power to which the local residents were submitted was $5.3 \cdot 10^{-3}$ W/m2 which is quite high with regards to the figures in Table 1. Therefore the residents were initially submitted to a strong pro-cancer effect due to the constant background power emitted by the GSM base station. T cells which were controlling cancer lost control at the onset of the GSM base station due to the transition to the constant GSM background, causing the observed high number of cancer cases one year after the base station was turned on.

Replacement of these T cells by other lines of T cells may have been speeded up by the permanent anti-cancer effect owed to the time variations of the GSM signal (i.e. day/night variations, for example). But this speeding up may have been inefficient in the vicinity of the base station for the following reasons:

- a relatively strong power was applied yielding a strong GSM constant background (persons residing near GSM base stations always withstand a notably higher power than the general population).

- the production of T cell precursor in the bone marrow is not expected to be affected by the artificial waves.

- due to the strong attenuation of the W_{dest} by the constant background there may not have been any T cell precursor capable of surviving T cell positive selection in the presence of the GSM background amongst those T cell precursor yielding T cells affected by GSM. There were obviously T cell precursors yielding T cells un-affected by GSM (due to appropriate Δ_b values) and these un-affected T cells could probably replace some of those T cells which had lost control of existing neoplasms. But the thymus output of such T-cells un-affected by GSM was also un-affected by the anti-cancer effects of GSM.

- the above-mentioned lack of T cell precursors depends on the strength of the GSM background. It is thus expected that a threshold power exists for the GSM background, above which no significant anti-cancer effect due to an additional time-variable signal within the GSM frequencies can be observed. Residents submitted to an above-threshold GSM background power are thus expected to be deprived of GSM anti-cancer effects whilst at the same time submitted to a strong transitional pro-cancer effect following onset of the base station.

Therefore it is likely that no significant anti-cancer effect related to GSM time variations exists for persons permanently residing in the immediate vicinity of GSM base stations. Whether or not residents of the immediate vicinity of the base station studied in [47] could benefit from any anti-cancer effects due to GSM time variations, it was insufficient to avoid cancer in this specific case.

In [47] most cancer victims were women. This is somewhat surprising in view of the fact that in Paris in 2006 the reaction to DVB onset was stronger in men. [47] does not give any indication as to the professional occupations of victims, but a potential explanation for the unusual sex ratio may be a higher number of non-working women or of women working and living in the same exposed area, as compared to the number of non-working men or men working and living in the exposed area. Persons who work outside the exposed area have a part time low exposure during which the immune response remains efficient, which brings their case towards Table 2 column E corresponding to an anti-cancer effect.

Thus the observations in [47] are thus fully in agreement with the present theory.

13 interpretation of the increase of cancer incidence rate in certain cell phone users

In [23] a strong and significant increase of brain cancer incidence was found for short-term heavy users of mobile

phones. In [27] a comparable increase is confirmed for users of both digital (GSM) and analog (NMT) mobile phones that have a high number of cumulative hours of exposure. The result in [23] is dominated by GSM users. In [27] in the case of analog cellular phone users it is also shown that there is a significant increase of brain cancer incidence for latencies superior to 20 years, the increase becoming even more significant after 25 years. Since the most ancient users also tend to have the largest cumulative hours of exposure, the increase in [27] for the case of analog phone users is most likely in relation with the time since first use, rather than the "intensity" of phone use. Therefore, increases for GSM and analog users seem to have different characteristics:

- for users of GSM phones, there is an increase of brain cancer incidence in relation to the intensity of phone use (i.e. hours per year), probably with also a minimum threshold for cumulative hours.

- for users of analog phones there is an increase of brain cancer incidence in relation with the time since first use, which becomes significant only after about 20 to 25 years.

Therefore, I propose a different interpretation for each of these increases.

13.1 long term increase of cancer incidence in users of analog cellular phones

I consider an analog cellular phone user having a developing neoplasm when he is relatively young, say younger than 40. This analog phone user benefits from an anticancer effect of the analog cellular phone so that a line of T cells is generated which controls brain cancer, whilst in the same situation a non-user of analog phone would immediately have developed brain cancer and probably died. Now this does not necessarily eliminate the neoplasm: the neoplasm survives, and the T cell line keeps controlling it so that the neoplasm does not reach a detectable size. 25 years later, the T cell line in question may reach the end of its lifespan or at least have a reduced reproduction rate. Thus the neoplasm gets out of control. The patient is most likely aged more than 60. He no more benefits from the anti-cancer effect of analog phones. His immune system is generally weaker than at a younger age. He is unable to produce a new line of T cells able to control the neoplasm again. He is thus diagnosed with brain cancer.

Thus, the cumulative increases of brain cancer for old patients who at a younger age were able to control their brain cancer only due to the anticancer effect of analog phones may be the underlying cause for the statistically observable increase of the cancer death rate for latencies of more than 20 years in [27]. This increase would thus be the counterpart of an earlier decrease.

13.2 short term increase of cancer incidence in heavy users of GSM phones

The pro-cancer effect of intense GSM use is short term and is therefore unrelated to any exhaustion of a previous anticancer effect. It is further unrelated to any direct effect as per Table 2 which does not predict such a pro-cancer effect. Further, there is no indication that this short-term effect exists for analog cellular phones or CDMA cellular phones, which do not use a pulsed wave.

I propose that this pro-cancer effect of intense GSM use may be related to the basic mechanism described in section 4 and possibly to the direct mutagenic effect described in section 4.7.

It was shown in section 4 that a pulsed wave can induce a conformational change of an elementary biological system. The existence of such conformational change was experimentally confirmed for exposure to a single GSM phone at $0.1W/m2$ which is about 100 times less than the maximum authorized power to which the brain can be exposed during a call. Such conformational change may cause cancer indirectly, for example if it affects a protein implied in DNA replication.

Alternatively, the direct mutagenic effect described in section 4.7 may have caused this pro-cancer effect.

Thus, the basic principle discussed in section 4 gives rises to different detailed mechanisms which could potentially explain a pro-cancer effect of the pulse train of a single GSM phone. But in any case this pro-cancer effect of a GSM pulse train would be caused by a direct or indirect mutagenic action rather than an action on the immune system.

14 Conclusions

The essential teaching of this paper is a general framework for explaining at least certain effects of artificial electromagnetic waves on biological systems. This framework can be summarized as follows:

- Stimulated transitions occur between different conformations of elementary biological systems.

- Such transitions can be stimulated either by the thermal electromagnetic field or by an artificial electromagnetic wave.

- The interplay between transitions stimulated by the thermal electromagnetic field and transitions stimulated by artificial electromagnetic waves may explain a number of effects of artificial electromagnetic waves on biological organisms.

One example of a mechanism within the general framework, described in section 4 and based on transitions between two conformations, was chosen because its features make it quite obvious that it is explainable only through quantum mechanics. The other example involving the TCR-pMHC system, based on transitions between three conformations, was chosen because of its public health consequences and because existing knowledge of the TCR-pMC interaction made it easier to develop the concept. It is expected that other biological effects of artificial electromagnetic waves should be explainable within this framework.

In the specific case of the TCR-pMHC interaction a complete model was developed. Essential qualitative predictions depend only on fundamental features of the model. The full model yields an improved understanding and quantitative analysis of the phenomena but is far from complete. Future theoretical and experimental work may focus on improving this model, including further refining

the model, obtaining essential model parameters which as of today are not known with any reasonable precision, and obtaining further experimental confirmations. One aspect which is of particular interest is to better identify the conformations of the TCR-pMHC which are implied the herein described interaction mechanism.

The finding that artificial electromagnetic waves interact with biological systems based on a combination of thermally stimulated transitions and transitions stimulated by the artificial electromagnetic wave is believed to be the underlying cause of many biological effects of artificial electromagnetic waves.

With respect to cancer, the detailed theory of the TCR-pMHC interaction explains apparent contradictions between observed increases of cancer incidence near transmitters [47] [6], decrease of brain cancer incidence in certain cellular phone users [23] [42], and global decrease of cancer incidence since the generalization of communication networks using time-variable electromagnetic waves (figure 29). The reason why the pro-cancer effects of radio or television electromagnetic waves have not been consistently demonstrated in earlier work [20] [21] [6] [14] [28] is most likely because statisticians expected a permanent effect, whilst the pro-cancer effect is in essence transient. The basic mechanism of stimulated transition between two conformations may further explain observed increases of brain cancer incidence in heavy GSM users [23] [27] which are not explainable by the theory of the TCR-pMHC interaction.

The theory of the TCR-pMHC interaction is not limited to cancer. It predicts effects on most diseases. Future work may comprise a validation of the theory's predictions on diseases other than cancer.

The theory presented herein has therapeutical implications with respect to cancer. The anti-cancer effect of temporary exposure to electromagnetic waves [33] is now understood. A treatment for cancer should ideally combine a permanent stay in a Faraday cage to interrupt any ongoing transient pro-cancer effect and to create a transient anti-cancer effect, and temporary exposures to electromagnetic waves to create an anti-cancer effect as previously known [33]. Ideally, the operating physician and the neighbourhood should be protected from the electromagnetic waves used for any treatment of cancer, so as to avoid the development of any auto-immune diseases caused by the same temporary exposure which cures cancer.

It is also hoped that the rational understanding of the non-thermal effects of electromagnetic waves, which is provided herein, will open the way for fundamental changes in the manner electromagnetic waves are being used.

References

[1] *Avis de déces*. www.avis-de-deces.net.

[2] *dipole moments server*. http://dipole.weizmann.ac.il.

[3] *Protein Data Bank*. www.rscb.org/pdb.

[4] *patent number FR 732.276*, 1932.

[5] effect of counterions on the spectrum of dissolved dna polymers. *physical review A*, 45(10):7610–20, may 1992.

[6] Decreased survival for childhood leukemia in proximity to television towers. *Archives of Environmental Health*, 58(9):560–564, 2003.

[7] Bioinitiative report: a rationale for a biologically-based public exposure standard for electromagnetic fields (elf and rf). Technical report, Bioinitiative Working Group, 2007.

[8] Mise jour de l'expertise relative aux radiofréqeunces, saisine no 2007/007. Technical report, Agence Francaise de sécurité sanitaire de l'environnement et du travail, 2009.

[9] R K Adair. Criticism of lednev's mechanism for the influence of weak magnetic fields on biological systems. *Bioelectromagnetics*, 13:231–235, 1992.

[10] Agence Nationale des Fréquences, www.cartoradio.fr.

[11] T Kerselaers B Sacco. *The Lakhovsky Multiple Wave Oscillator Secrets Revealed*. http://users.skynet.be/Lakhovsky.

[12] C F Blackman, S G Benane, D E House, and D J Elliott. Importance of alignment between local dc magnetic field and an oscillatig magnetic field in responses of brain tissue in vitro and in vivo. *Bioelectromagnetics*, 11:159–167, 1990.

[13] J P Blanchard and C F Blackman. Clarification of an ion parametric resonance model for magnetic field interactions with biological systems. *Bioelectromagnetics*, 15:217–238, 1994.

[14] R A Cartwright. Cancer and tv towers: association but not causation. *MJA*, 165(2):599–600, december 1996.

[15] CepiDc-Inserm (Centre d'Epidemiologie sur les Causes Medicales de Deces, Institut National de la Sante et de la Recherche Medicale), www.cepidc.inserm.fr. *indicateurs de mortalite*.

[16] C. Cohen-Tannoudji, B. Diu, and F.Laloe. *Mecanique quantique*. Hermann, 1998.

[17] D. Q. Colby and S.M.Prusiner. Prions. In *Cold Springs Harbor Perspectives in Biology*. 2011.

[18] F P de Gannes, M Taxile, S Duleu, A Hurtier, E Haro, M Geffard, G Ruffi, B Billaudel, P Leveque, P Dufour, I Lagroye, and B Veyret. A confirmation study of russian and ukrainian data on effects of 2450 mhz microwave exposure on immunological processes and teratology in rats. *Radiation Research*, 172:617–624, 2009.

[19] L.H. Margaritis D.J.Panagopoulos, E. D. Chavdoula. bioeffects of mobile telephony radiation in relation to its intensity or distance to the antenna. *Int. J. Radiat. Biol.*, 86(5):345–357, may 2010.

[20] H Dolk, G Shaddick, P Walls, C Grundy, B Thakrar, I Kleinschmidt, and P Elliott. Cancer incidence near radio and television transmitters in great britain: Sutton coldfield transmitter. *American Journal of Epidemiology*, 145(1):1–9, january 1997.

[21] H Dolk, G Shaddick, P Walls, B Thakrar, and P Elliott. Cancer incidence near radio and television transmitters in great britain - all high power transmitters. *American Journal of Epidemiology*, 145(1):10–17, january 1997.

[22] Yury G Grigoriev, Oleg A Grigoriev, A A Ivanov, A M Lyaginskaya, A V Merkulov, N B Shagina, V N Maltsev, P Leveque, d V A Osipov A M Ulanova a, and A V Shafirkin. Confirmation studies of soviet research on immunological effects of microwaves: Russian immunological results. *Bioelectromagnetics*, 31:589–602, 2010.

[23] The Interphone Study Group. Brain tumour risk in relation to mobile telephone use: results of the interphone international case-control study. *International Journal of Epidemiology*, 39:675–694, 2010.

[24] W. Grundler, F Kaiser, F Keilman, and J Walleczek. Mechanisms of electromagnetic interaction with cellular systems. *Naturwissenschaften*, 79:551–559, 1992.

[25] J. Scott Hale, T.E. Boursalian, and P.J.Fink G.L.Turk. Thymic output in aged mice. *PNAS*, 103(22):8447–52, 2006.

[26] M N Halgamuge, B R R Perssont, L G Salford, P Mendis, and J Eberhardt. Comparison between two models for interactions between electric and magnetic fields and proteins in cell membranes. *Environmental Engineering Science*, 26(10):1473–1480, 2009.

[27] L Hardell, M Carlberg, F Soderqvist, and K Hansson Mild. Case-control study of the association between malignant brain tumors diagnosed between 2007 and 2009 and mobile and cordless phone use. *international journal of oncology*, September 2013. doi: 10.3892/ijo.2013.2111.

[28] Bruce Hocking, Ian Gordon, H L Grain, and G E Hatfield. Cancer incidence and mortality and proximity to tv towers. *MJA*, 165(2):601–605, december 1996.

[29] P D Inskip, R E Tarone, E E Hatch, and P D Timothy et al. cellular-telephone use and brain tumors. *The New England Journal of Medicine*, 344(2):79–86, january 2001.

[30] C Johansen, J D Boice, J K McLaughlin, and J H Olsen. Cellular telephones and cancer: a nationwide cohort study in denmark. *Journal of the National Cancer Institute*, 93(3):203–206, february 2001.

[31] A V Kabanov, V M Komarov, and V Perez. The mechanism of accumulation of the large electric dipole moment in dna molecule. pm3 quantum-chemical analysis. *biofizika*, 50(3):434–443, 2005.

[32] A Lakhola, A Auvinen, M J Schoemaker, H C Christensen, M Feychting, C Johansen, L Klaeboe, A J Swerdlow, T Tynes, and T Salminen. Mobile phone use and risk of glioma in 5 north european countries. *International Journal of Cancer*, 120:1769–1775, 2007.

[33] Georges Lakhovsky. *Radiations and Waves, Sources of Our Life*. Emile L Cabella, 288 East 45th Street, New York, 1941.

[34] V V Lednev. Possible mechanism for the influence of weak magnetic fields on biological systems. *Bioelectromagnetics*, 12:71–75, 1991.

[35] S. McClory, Tiffany Hughes, Aharon G. Freud, Edward L. Briercheck, C. Martin, A.J.Trimboli, J. Yu, X. Zhang, G. Leone, G. Nuovo, and M.A.Caligiuri. Evidence for a stepwise program of extrathymic t cell development within the human tonsil. *J. Clin. Invest.*, 122(4), 2012.

[36] S Mieda and M Aida. Dipole moments of amino acid residues, gly and ala, in alpha-helix: Quantum chemical building blocks for macropole moment of alpha-helical polypeptide. *Chem. Lett.*, 41:1579–1580. doi:10.1246/cl.2012.1579.

[37] M.O.Scully and M. Suhail Zubairy. *Quantum optics*. Cambridge university press, 1997.

[38] J E Muscat, M G Malkin, S Thompson, S D Stellman, D McRee, A I Neugut, and E L Wynder. Handheld cellular telephone use and risk of brain cancer. *JAMA*, 284(23):3001–3007, December 2000.

[39] D J Panagopoulos, N Messini, A Karabarbounis, A L Philippetis, and L H Margaritis. A mechanism for action of oscillating electric fields on cells. *Biochemical and Biophysical Research Communications*, 272:634–640, 2000.

[40] P.H.Puech, D. Nevoltris, P. Robert, L. Limozin, C. Boyer, and P. Bongrand. Force measurements of tcr/pmhc recognition at t cell surface. *PLoS ONE*, 6(7), july 2011.

[41] J L Portes. *la vie et l'oeuvre de Georges Lakhovsky*. PhD thesis, Université Pierre et Marie Curie - facult de mdecine Piti-Salptrire, 1983.

[42] J. Schuz, R Jacobsen, J H Olsen, J D Boice Jr, J K McLaughlin, and C Johansen. Cellular use and cancer risk: Update of a nationwide danish cohort. *Journal of the National Cancer Institute*, 98(23):1707–1713, december 2006.

[43] S Takashima. Dielectric dispersion of dna. *journal of molecular biology*, 7:455–467, 1963.

[44] C Tanchot, F A Lemonnier, B Pérarnau, A A Freitas, and B Rocha. Differential requirements for survival and proliferation of cd8 naive or memory t cells. *science*, 276(5321):2057–2062. doi: 10.126/science.276.5321.2057.

[45] Hirotake Tsukamoto, K Clise-Dwyer, G E Huston, D K Duso, A L Buck, L L Johnson, L Haynes, and S L Swain. Age-associated increase in lifespan of nave cd4 t cells contributes to t cell homeostasis but facilitates devlopment of functional defects. *PNAS*, 106(43):18333–18338, 2009. doi/10.1073/pnas.0910139106.

[46] J A Verheugen and H P Vijverberg. *Cell Calcium*.

[47] R Wolf and D Wolf. Increased incidence of cancer near a cell-phone transmitter station. *International Journal of Cancer Prevention*, 1(2), april 2004.